POST-PROCESSING OF LOW DOSE

MAMMOGRAPHY IMAGES

THESIS

Jesung Kim, First Lieutenant, USAF

AFIT/GE/ENG/02-35

DEPARTMENT OF THE AIR FORCE
AIR UNIVERSITY
AIR FORCE INSTITUTE OF TECHNOLOGY

Wright-Patterson Air Force Base, Ohio

APPROVED FOR PUBLIC RELEASE; DISTRIBUTION UNLIMITED.

The views expressed in this thesis are those of the author and do not reflect the official policy or position of the United States Air Force, Department of Defense, or the U. S. Government.

AFIT/GE/ENG/02-35

POST-PROCESSING OF LOW DOSE MAMMOGRAPHY IMAGES

THESIS

Presented to the Faculty

Department of Electrical and Computer Engineering

Graduate School of Engineering and Management

Air Force Institute of Technology

Air University

Air Education and Training Command

In Partial Fulfillment of the Requirements for the

Degree of Master of Science in Electrical Engineering
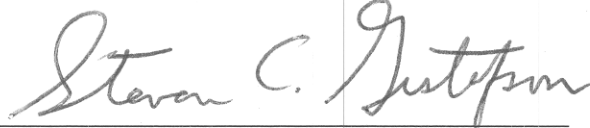
Jesung Kim, BS

First Lieutenant, USAF

May 2002
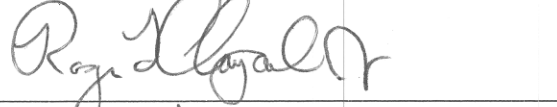
APPROVED FOR PUBLIC RELEASE; DISTRIBUTION UNLIMITED.

POST-PROCESSING OF LOW DOSE MAMMOGRAPHY IMAGES

Jesung Kim, BS
First Lieutenant, USAF

Approved:

Steven C. Gustafson (Chairman)		30 July 2002
		date
Roger L. Claypoole, Jr. (Member)		9 AUG 2002
		date
Eric P. Magee (Member)		9 AUG 2002
		date

Acknowledgments

I would like to express my sincere appreciation to my faculty advisor, Dr. Steven Gustafson, for his guidance and support throughout the course of this thesis effort. The insight and experience was certainly appreciated. I would, also, like to thank my sponsor, Lt Col William Ruck, from the Wright-Patterson AFB Hospital Radiology Department for the opportunity to work for him on this research. In addition, I am thankful for the advice and technical expertise bestowed upon me by Maj Roger Claypoole and Maj Eric Magee. Their support made my research possible. I thank Dr. Richard Mitchell for scanning the mammography film for the research at hand. My gratitude goes to Lt Col John O'Hair for both the support and latitude provided to me in this endeavor. I thank Dr. Michael Temple for his stewardship and endearing support. Finally, I would like to express my deepest gratitude to the Dayton Area Graduate Studies Institute for providing the means to an end in my efforts at AFIT.

Jesung Kim

Table of Contents

AFIT/GE/ENG/02-35

Abstract

In mammography, X-ray radiation is used in sufficient doses to be captured on film for cancer diagnosis. A problem lies in the inherent nature of X-rays to cause cancer. The resolution of the images obtained on film is directly related to the radiation dosage. Thus, a trade off between image quality and radiation exposure is necessary to ensure proper diagnosis without causing cancer. A possible solution is to decrease the dosage of radiation and improve the image quality of mammograms using post-processing methods applied to digitized film images. Image processing techniques that may improve the resolution of images captured at lower doses include crispening, denoising, histogram equalization, and pattern recognition methods. The Wright Patterson Air Force Base Hospital Radiology Department sponsored this research and provided digitized images of the American College of Radiology (ACR) phantom, which is a model for mammogram image quality and classification. Side by side comparisons were performed of high dose images and low-dose images post-processed using the methods mentioned. The result was improved-resolution mammography images for lower radiation doses. Thus, this research represents progress towards solving a problem that currently plagues mammography: exposure of patients to high doses of cancer-causing radiation to obtain quality mammography images. By improving the image quality of mammography images at lower radiation doses, the problem of cancer induced by high radiation exposure is alleviated.

POST-PROCESSING OF LOW DOSE MAMMOGRAPHY IMAGES

1. Introduction

The National Cancer Institute recommends that women from the ages 40 to 69 undergo breast cancer screening yearly (18:1). Screening mammography uses X-rays to detect abnormalities in women who have no palpable signs of breast cancer. In addition, women with unusual breast conditions such as lumps, pain, thickening, nipple discharge, or variations in breast size or shape can undergo diagnostic mammography. Diagnostic mammography can also be applied to evaluate any changes detected in a screening mammography. Screening and diagnostic mammography in conjunction with clinical breast exams (conducted by professional health care providers) stand as the best methods of detecting breast cancer as early as possible. However, with the benefits come possible side effects.

In mammography, X-ray radiation is used in sufficient doses to be captured on film for cancer diagnosis. A problem lies in the inherent nature of X-rays to cause cancer and in the fact that the resolution of the images obtained on film is directly related to the radiation dosage. Thus, a trade off between image quality and radiation exposure is necessary to ensure proper diagnosis without causing cancer.

A possible solution is to decrease the dosage of radiation and improve the image quality of the mammography using post-processing methods applied to digitized film images. Image processing techniques that may improve the image resolution captured at

lower doses include edge detection, denoising, histogram equalization, and pattern recognition methods. The Wright Patterson Air Force Base Hospital Radiology Department sponsored this research. This department provided digitized mammograms of the ACR phantom, which is a model for image quality and classification of mammograms. In addition, the department provided supervised access to the mammography machines and associated resources such as technical literature and user manuals.

This research addresses a problem that currently plagues mammography: exposure of patients to high doses of cancer causing radiation to obtain quality mammography images. By improving the image quality of the mammography images at lower doses of radiation, the problem of cancer induced by high radiation exposure is alleviated. This could lead to changes in the way that mammography is administered, resulting in a safer diagnostic procedure and a lower percentage of patients developing breast cancer.

2. Background

2.1 Review of relevant mammography technology

Mammography focuses X-rays on breast tissue, and the X-rays attenuate as they pass through varying densities. The resulting attenuated X-rays expose film, leading to the mammography image. The abnormal cancerous tissue attenuates the X-rays substantially more than the fatty storage and fascia that surrounds active breast tissue (2:2). Early comparisons of mammography images of cancer tissue with gross (visible to

the naked eye) and microscopic anatomy led to the observation of small black spots. The discovery of those spots represents the first demonstration of microcalcification detection (11:9). Microcalcifications are minute regions of hardened tissue resulting from the impregnation of calcium deposits (21).

As research progressed in mammography, the medical community recognized a radiographic differentiation of benign, or non-cancerous, and malignant, or cancerous, breast lesions. Spiculated, or needle-like, lesions proved to be a sign of malignancy, whereas well-circumscribed lesions indicated benign cases (11:39). With advances in technology and more mammography data, breast radiography evolved from an art into a science that distinguished between normal breast tissue, microcalcifications, and spiculated lesions (11:9).

As mammography gained in popularity, a need for standardization surfaced. The American College of Radiology (ACR) initiated the Mammography Accreditation Program to fulfill this requirement. The program has the following goals: 1) To establish quality standards for mammography, 2) to provide a mechanism for mammography sites to compare voluntarily their own performance with national standards, 3) to encourage quality assurance practices in mammography, and 4) to ensure reproducible high quality images at low radiation doses to the patient (11:138). The research reported here is largely concerned with the first and last goals because the goal is to reduce the dosage of X-rays while maintaining high image quality and to compare the reduced image results using a standardized metric.

The ACR phantom image evaluation of the entire mammographic imaging chain represents one quality control measure required for accreditation.   The mammographic

imaging chain includes: X-ray equipment, techniques factors, image receptors, and processing. The evaluation involves the analysis of a test phantom that consists of objects that simulate masses and microcalcifications.   Figure 1 shows an ACR phantom.
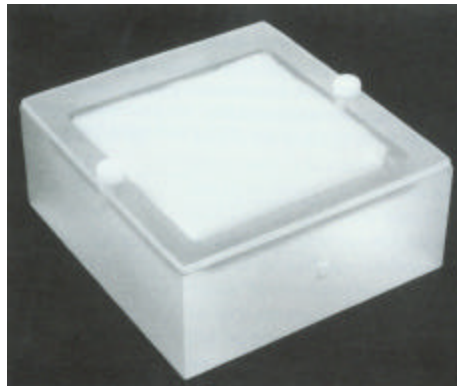

Figure 1 American College of Radiology (ACR) phantom, a test object that simulates masses and microcalcifications. The ACR phantom is used as a standard measure of the image chain performance of mammography systems (10:166).

 In order to test the imaging chain, a trained medical physicist evaluates the mammography image of the ACR phantom using a standardized scoring methodology. For accreditation, the criteria are as follows: the three largest microcalcification groups with speck diameters of 0.54 mm and the three largest masses with thickness of 2.0 mm must be demonstrated (11:139). Typically, the simulated microcalcifications are grouped as the vertices of a pentagon, to allow for precise mensuration, while dime-sized disks serve as the simulations for the masses. The application of the ACR phantom is not limited to accreditation purposes but can also be used as a metric in experimental research to improve the imaging chain, precluding the need for human test cases.

Research in improving the imaging chain focuses on current priorities for improved breast cancer imaging. The priorities include: 1) contrast enhancement, 2)

scatter control, 3) and noise reduction (11:101). Contrast is the most important feature in mammography in detecting subtle abnormalities. Regardless of signal to noise ratios, some objects below a certain contrast threshold are not detectable. Two factors contribute to the contrast in mammographic images: subject contrast and recording system contrast. Subject contrast is affected by X-ray dosage and the scattering properties of the breast. Lower doses of X-rays lead to lower contrast images. Recording system contrast is dependant on the characteristics of the mammographic film and the process by which the film is developed (11).

2.2 Review of relevant image point processing techniques

In order to alleviate the contrast problem, histogram modification and edge enhancement techniques can be employed. The histogram of an image is a representation of "the relative frequency of occurrence of the various gray levels in the image" (12:241). Thus, low contrast images possess narrow histograms while high contrast images have more uniform histograms. Since increasing contrast is a goal, a method to stretch the histograms of low contrast mammography images is desired. For this purpose, "Histogram modification techniques are attractive due to their simplicity and speed, and have achieved acceptable results for some applications" (1:163).

Under the genre of image enhancement, point processing techniques such as contrast modification and histogram equalization are employed to enhance image detail. The empirical histogram P of an image $a[m,n]$ quantized to reconstruction levels $\{r_1, r_2, \ldots r_L\}$ is

$$P_a(r_I) = \frac{N(r_i)}{M}$$

where $N(r_i)$ is the total number of pixels in the image which take on value r_i and M is the

total number of pixels in the image. The histogram represents an approximation of the

probability density function (PDF) of gray levels in an image. Low contrast images

result in histograms that are "peaky", whereas high contrast images have histograms that

are spread out. In the application of contrast modification, a non-linear function is

applied to each pixel in order to vary the output contrast and histogram (See Figure 2).

Typically, the objective is to mimic a high contrast image by spreading a "peaky"

histogram by multiplying the pixels corresponding to the "peaky" portion of the

histogram by a high slope. If the slope is steep, the output histogram will be stretched

more than if the slope is less steep.
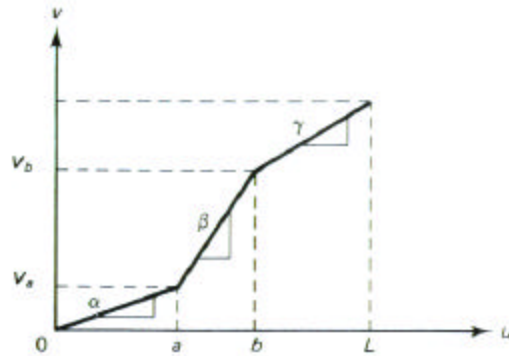
Figure 2 Non-linear function to perform contrast stretching. Here u represents the given
pixel gray level and v is the mapped output pixel gray level. The variables **a**, **b**, and **g**
represent the slopes of the transformation function respectively, L represents the
maximum given pixel gray level, and a and b represent the variable parameters for the
start and finish of the region of stretching (11:235).

By multiplying each pixel by this non-linear function, the histogram becomes stretched

(See Figure 3).

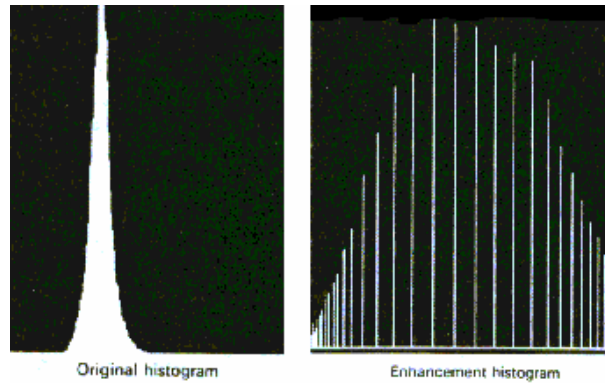Original histogram   Enhancement histogram

Figure 3 Original histogram is from the original image and enhancement histogram is from the image after contrast stretching. Contrast stretching spreads a "peaky" histogram by multiplying the pixels corresponding to the "peaky" portion of the histogram by the high slope portion of the non-linear function (11:236).

The enhanced images have high contrast, giving the appearance that areas that are

expected to be dark are darker, and areas that are light are lighter (See Figure 4).

Originals   Enhanced

Figure 4 Original and enhanced image with contrast stretching (11:236).

In histogram equalization, the goal is to obtain a uniform histogram for the output image.

Histogram equalization uses an automated contrast modification scheme. Given $P_r(r)$,

obtaining $S = T(r)$ such that $P_s(s)$ is uniform, requires:

$$S_k = T(r_k) = \sum_{i=0}^{k} P_r(r_i)$$

15

This function automatically maps out a new histogram for the image to be enhanced. The enhanced image now has a high contrast histogram. As a result, details lost in dark regions are brought out (See Figure 5).
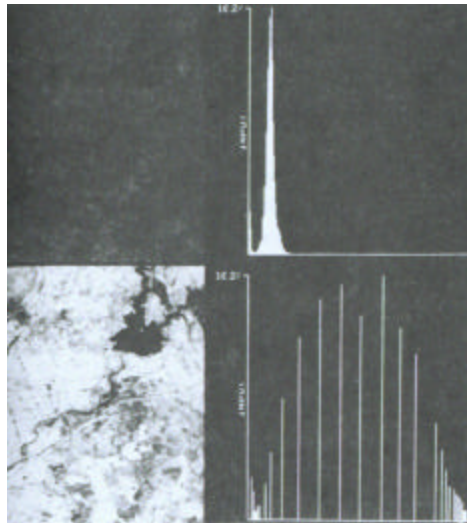
Figure 5 At the top left-hand corner is the original image with its corresponding histogram to its right. The bottom left-hand image is the enhanced image with histogram equalization and its corresponding histogram. Histogram equalization performs contrast stretching in an automated fashion (11:243).

In terms of improving contrast, histogram equalization serves as an effective technique because of its automated capacity to make the histogram of the output image more uniform, making this method simple and fast while improving image contrast.

2.3 Review of relevant image edge enhancement techniques

Radiation scatter remains a problem in mammography, however, the contribution of scatter is more evident when X-ray dosage is decreased. Scatter is signal dependant noise that creates images with nonuniform illumination, when contrast decreases from the

epicenter of the X-ray focus. In addition, blurring of the mammography image occurs

due to scattering (11:73). Current research focuses on edge sharpening methods to

reduce the deleterious effects of scattering. Unsharp masking stands as a powerful

enhancement algorithm to counter scattering. The low pass filtered, unsharp version of

an image is subtracted from the original image in unsharp masking, which "sharpens

edges by subtracting a portion of the Laplacian filtered component from an original

image" (1:164). Also, unsharp masking "is equivalent to adding the gradient, or a high-

pass signal, to the image" (12:249). This linear operation is represented by the following,

$$v(m,n) = u(m,n) + \lambda g(m,n)$$

where $v(m,n)$ is the enhanced image, $u(m,n)$ is the original image, the gain coefficient $\lambda >$

0 , and $g(m,n)$ is a suitably defined gradient at (m,n) (12:249). A desirable function is the

discrete Laplacian operator (See Figure 6).
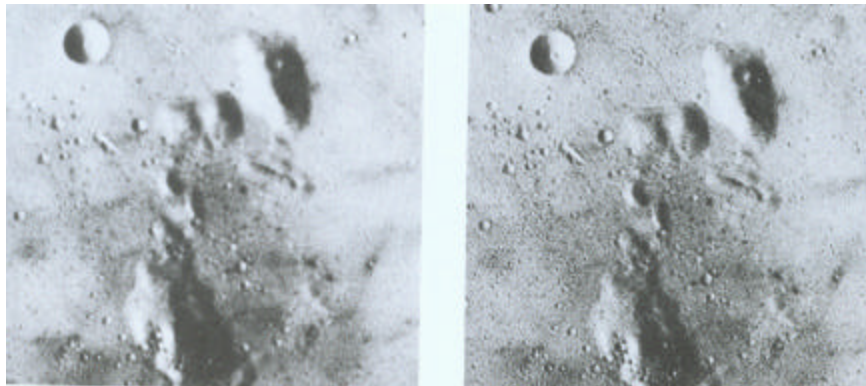
Figure 6 The figure to the left is an image of the surface of the moon. Using unsharp
masking with a discrete Laplacian operator, the original image is enhanced to yield the
image to the right. Unsharp masking sharpens edges by subtracting a portion of the
Laplacian filtered component from an original image (11:251).

Unsharp masking is an effective method for enhancing the image quality of mammography images.

However, this technique is limited by its linear and single scale properties and is "less effective for images containing a wide range of salient features typically found in digital mammography." The application of the redundant discrete wavelet transform (RDWT) (See Figure 7) has been recommended because of its connection to traditional techniques of unsharp masking (1:164). In Figure 7, the two levels to the top $\hat{g}\,(\omega_x)$ and $\hat{g}\,(\omega_y)$ represent the forward filters for the high resolution channel of this stage and $\hat{k}\,(\omega_x)\hat{l}\,(\omega_y)$ and $\hat{l}\,(\omega_x)\hat{k}\,(\omega_y)$ are the inverse filters. In the bottom level, $\hat{h}\,(\omega_x)\hat{h}\,(\omega_y)$ represents the forward filter for the low resolution channel for this stage. The $\hat{g}\,(2\omega_x)$ and $\hat{g}\,(2\omega_y)$ represent the forward filters for the high resolution level of the next stage down with its inverse filters to the right of them. In the bottom level of the next stage down, $\hat{h}\,(2\omega_x)\hat{h}\,(2\omega_y)$ represents the forward filters for the low resolution with its inverse filter to the right of it. The high resolution channels can be enhanced while discarding the low resolution channels.
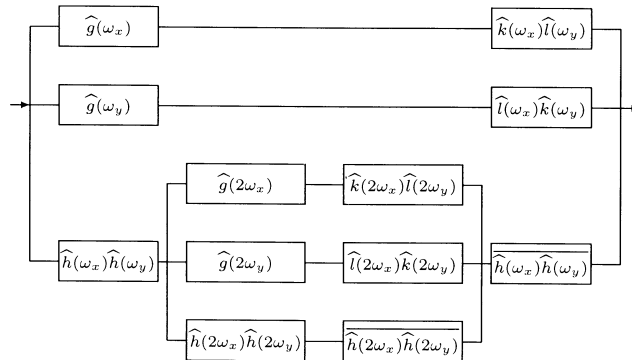
Figure 7 Two-dimensional Redundant Wavelet Transform (RDWT) with two levels shown. The RDWT is used to discard several channels of lower resolution, while enhancing channels confined to higher frequencies (1:182).

By considering two special cases of linear enhancement, it can be shown that a RDWT framework for enhancement includes unsharp making with a Gaussian low-pass filter (1:171). For the first case, transform coefficients of channels $0 \pounds m \pounds N - 1$ are enhanced by the same gain $G_0 > 1$. The input and output relationship of an unsharp masking system is

$$s_e(l) = s(l) + (G_0 - 1)[s(l) - (s * c_N)(l)],$$

where c_N is approximately a Gaussian low-pass filter (Wavelets:172). The second case maintains transform coefficients of a single channel p, where $0 \pounds p \pounds N$ are enhanced by a gain $G_p > 1$. The input and output relationship of an unsharp masking system is

$$s_e(l) = s(l) - (G_p - 1) \cdot \Delta(s * \mathbf{h})(l),$$

where $\mathbf{h}(l)$ represents the impulse response of an approximate Gaussian filter. The RDWT is flexible and versatile to allow for the inclusion for these two types of unsharp masking systems. Although highly effective in sharpening images, the RDWT with combined enhancement and denoising introduces artifacts that may become false positives in mammography images (or when mammograms are read as abnormal) when no cancer is actually present.

2.4 Review of relevant image noise reduction techniques

Noise in the form of random density fluctuations due to quantum noise is more apparent when X-ray dosage decreases. An additive noise model is

$$g(n_1, n_2) = f(n_1, n_2) + v(n_1, n_2),$$

where $v(n_1, n_2)$ is the signal-independent additive random noise, $f(n_1, n_2)$ is the signal of interest, and $g(n_1, n_2)$ is the signal with additive random noise. Examples of "additive

random noise degradation include electronic circuit noise, and in some cases amplitude quantization noise" (13:527). Sources of additive random noise in mammography images include the random absorption of X-ray quanta by the image receptor (11:65). Also, "Quantum noise can be characterized in terms of the standard deviation about the mean number of detected quanta, and this value is proportional to the square root of the mean number of quanta" (11:65). Thus quantum noise standard deviation is given by,

$$\boldsymbol{s} = \sqrt{N(E)\boldsymbol{h}(E)g(E)},$$

where g denotes the amount of light reaching the film per interacting X-ray quantum in the screen and $\boldsymbol{h}(E)$ is mean quantum efficiency (11:65). Another source of noise is radiation scatter, which is signal dependant. The radiation scatter noise can be modeled as blur due to its blurring effects in mammography images. Factors that influence this type of noise are the amount of scatter produced, its transport through the breast, the efficiency of the grid performance, and η of the screen for scatter absorption; these factors are dependant on the dosage of X-rays (11:66). The reduction of the X-ray dosage increases the contribution of scatter and, in turn, the noise.

Wiener filtering is one method for reducing additive random noise in images and may restore image in the presence of blur (13:527). Jain states that, "Wiener filtering is a method of restoring images in the presence of blur as well as noise" (12:276). The deblurring and denoising characteristics make Wiener filtering advantageous for the research reported here. One form of the Wiener filter is

$$H(\boldsymbol{w}_1, \boldsymbol{w}_2) = \frac{P_f(\boldsymbol{w}_1, \boldsymbol{w}_2)}{P_f(\boldsymbol{w}_1, \boldsymbol{w}_2) + P_v(\boldsymbol{w}_1, \boldsymbol{w}_2)},$$

where it is assumed that $f(n_1,n_2)$ and $v(n_1,n_2)$ are samples of zero-mean stationary random processes which are linearly independent of each other and that their power spectra $P_f(w_1, w_2)$ and $P_v(w_1, w_2)$ are known (13:527). However, the research at hand deals with both signal dependant and signal independent noise. The signal dependant scatter noise can be modeled as blur in the mammography image. A Wiener filter with deblurring characteristics can be designed to reduce the effects of scatter when modeled as blur instead of signal dependant noise. Wiener filtering achieves a compromise between a low-pass noise smoothing filter and a high-pass inverse filter as shown in Figure 8.
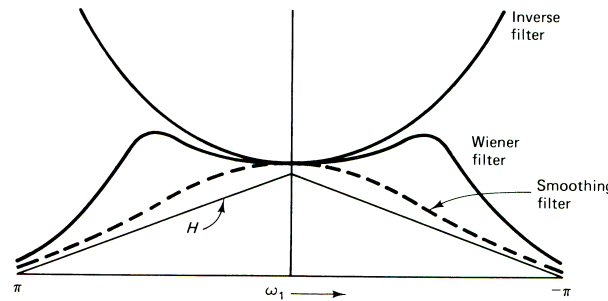
Figure 8 Wiener filter characteristics. The Wiener filter achieves a compromise between a low-pass noise smoothing filter and a high-pass inverse filter (11:280).

The low-pass smoothing filter and high-pass inverse filter characteristics of the Wiener filter form a band-pass filter. The frequency response of a Wiener filter shown in figure 8 illustrates that the Wiener filter is useful when blur and noise are present in an image. The characteristics of mammography images vary from one area to another. As a result, an adaptive filter that changes with the varying characteristics of the image and noise is desired. Pixel-by-pixel processing entails processing methods that take into consideration the local characteristics of the region centered around the pixel (13:534). Figure 9 provides an example of a adaptive Wiener filter processed image.
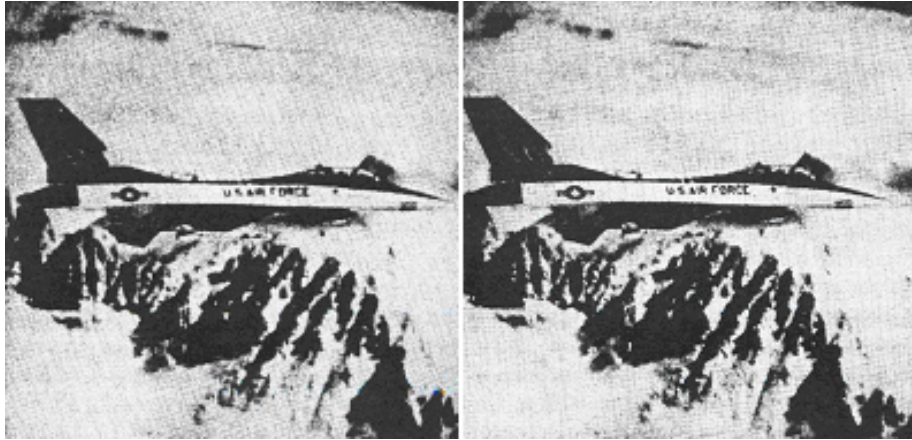
Figure 9 The image to the left represents the original image degraded by Gaussian noise, and the image on the right represents the adaptive Wiener filtered version of the image on the right. Wiener filtering achieves a compromise between a low-pass noise smoothing filter and a high-pass inverse filter (12:540).

As mentioned above, the RDWT is inherently set up for unsharp masking and denoising capabilities. The magnitude of the gradient coefficients are denoised first, followed by the enhancement of the sum of Laplacian coefficients. This method reduces the number of artifacts introduced by the RDWT method of image improvement. The RDWT is considered shift-invariant. As a result, artifacts such as those due to Gibbs phenomena are averaged out when using the RDWT. This averaging characteristic is known as cycle spinning. The RDWT method creates redundant sets of data functions to reconstruct an image. By taking into consideration all of the redundant data sets by applying denoising followed by inverse transforming and adding the results together, the RDWT performs cycle spinning (22:1). Consequently, the image is denoised with less artifacts apparent due to discontinuities. An example of the RDWT used for denoising and enhancement is shown in Figure 10.
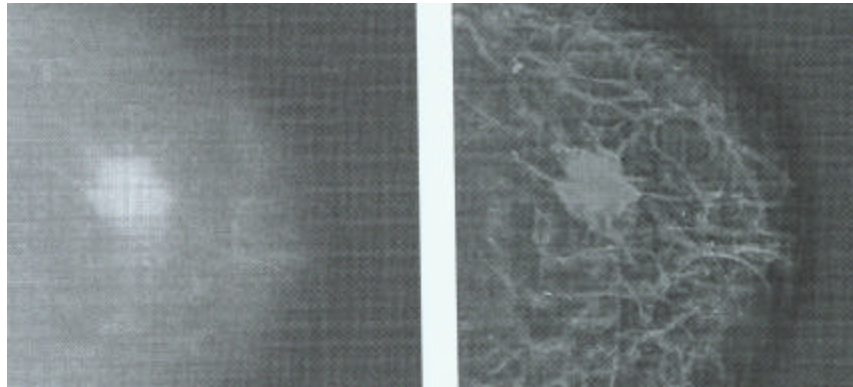
Figure 10 The image to the left is the original mammography image, and the image to the right is the denoised, enhanced image from the RDWT (1:185).

To aid in the Radiologist's goal of recognizing detail in mammography images, edge detection methods are employed, where an edge in an image is, "a boundary or contour at which a significant change occurs in some physical aspect of an image, such as the surface reflectance, illumination, or the distance of the visible surfaces from the viewer" (13:476). The research reported here is concerned with changes in the image intensity. Figure 11 diagrams an edge detection technique.
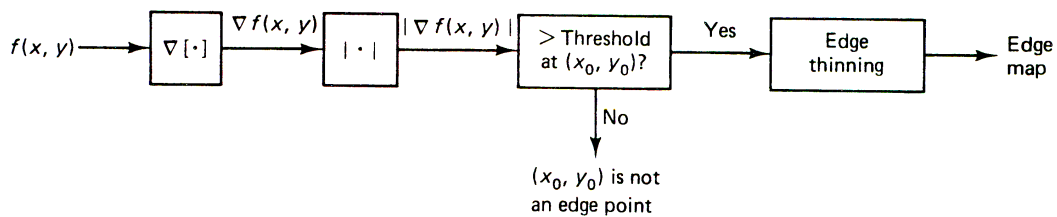
Figure 11 Gradient operator edge detection system. The gradient operator measures the gradient of the image to determine where edges occur (12:480).

The gradient of the image is taken and compared to a threshold to determine whether an edge is present or not. The edge thinning preserves the edge information and contributes to the edge map information. There are several types of gradient methods that can be used in edge detection. The Canny and Prewitt methods represent two types of gradient methods in edge detection. The Prewitt method uses the Prewitt approximation to the derivative to find edges where the gradient of the image is maximum. The Canny method finds edges at local maxima of the gradient of the image. By taking the derivative of the Gaussian filter, the gradient of the image is found. The Canny method differs from the Prewitt method in that the Canny method detects both weak edges and strong edges using two thresholds, whereas the Prewitt method only uses one threshold. The Canny edge detector accepts the weak edges if they are connected to the strong edges. As a result, the Canny method is more likely to detect true edges rather than noise.

2.5 Current research in mammography enhancement

Current research in medical image enhancement applies numerous image processing techniques that concentrate on mammography images captured at standard 150 mRad doses of X-rays. Pixel operations such as compensation for nonlinear characteristics of display or print media, intensity scaling, and histogram equalization are fundamental enhancement techniques used in mammography. The mammography images displayed on the Cathode Ray Tube (CRT) or on printed media have a nonlinear intensity profile when observed due to the nonlinear intensity characteristics of the display or printing mechanisms. A transform of the inverse of the display or printing mechanism's nonlinearity is applied to correct for the nonlinear attributes of the image

display. In order to characterize the display or printing mechanism's nonlinear intensity, a test image can be used to model the complete intensity scale of the image chain (2:5). This method is a problem that affects all medical imaging. A correction of nonlinear characteristics that stems from the mechanisms to procure the mammography images would be advantageous for the research at hand.

When the dynamic range of the mammography image data greatly exceeds the characteristics of the display system, intensity scaling can be applied to allow the observer to focus on specific intensity bands in the image. This is done by modifying the image so that the intensity bands of interest span the entire dynamic range of the display (2:5). This method would be practical if a priori information on the bands of interest is present. Since a priori information on the bands of interest of the mammography images captured at lower doses is not available, this method would not be applicable to the research at hand.

Histogram equalization is another fundamental pixel operation used in mammography to enhance images and does not require a priori information. This technique is used to make the histogram of an image more uniform over the available intensity band. This method is successful in increasing contrast in mammography images captured at 150 mRads, and would also be useful for the research at hand.

Local operator techniques such as noise suppression by median filtering is applied to enhance mammography images. In median filtering, a window is centered on each pixel *(m,n)* of the original image, and the median value within the window is obtained. The median value is then outputted as the value for the pixel with coordinates *(m,n)* that the window was centered on. This method is used to eradicate noise impulses with high

pixel values (2:7). For the research at hand, the median filter would not be beneficial since the microcalcifications that are of interest may have similar characteristics as impulsive noise. Microcalcifications are small and have high intensity values compared to their surroundings.

Adaptive image filtering techniques such as Wiener filtering and unsharp masking are applied to mammography images for enhancement in current research. The adaptive Wiener filter is used in current research since standard Wiener filters have limited success in image enhancement due to its low-pass filter characteristic. The adaptive Wiener filtering and unsharp masking has some success in enhancing mammography images at 150 mRads and would be useful in enhancing mammography images captured at lower doses.

Enhancement of mammography images is achieved by multiscale nonlinear operators in current research. The implementation of combined denoising and enhancement using the RDWT framework is the focus of current research. This method has promising success in improving local contrast for features in mammography images captured at 150 mRads. Using the RDWT with combined denoising and enhancement would also aid in enhancing the mammography images captured at lower doses. However, the artifacts that may arise due to the use of the RDWT makes it disadvantageous for the research at hand. Any artifacts can be misconstrued as objects of interest such as microcalcifications, fibers, or disks.

3. Methodology

3.1 Procedure for obtaining images

This research used the following methodology: 1) obtain mammography images of ACR phantoms at varying X-ray doses, 2) process the images using various image processing techniques, and 3) compare the results from the image processing techniques with the original images quantitatively and qualitatively. An experimental setup of the imaging system was required in order to procure images in a digital format compatible with the MATLAB processing environment. The following describes the procedure used to obtain the digitized images:

1) The imaging plate (IP) is placed inside a cassette and exposed using standard X-ray equipment.

2) The X-rays that pass through the ACR phantom and react with the IP, forming a latent image.

3) The latent image is read via laser scanning, which stimulates the IP so that it emits stored energy in the form of ultraviolet light.

4) This emission, known as Photostimulable Luminescence (PSL), is detected using a photomultiplier, and the light emission is converted to electrical signals.

5) These signals are reconstructed as a visual image on the computer screen and saved on a disk.

The procedure was used to obtain four images at varying doses: 1) 75 mRad, 2) 100 mRad, 3) 125 mRad, and 4) 150 mRad, designated Low dose, Low-medium dose, Medium-high dose, and High dose, respectively. JPEG compression was used to save the

images. This form of compression in not ideal for the research at hand, however, it

allows for a media that is compatible with the MATLAB 6.0 workspace environment.

The JPEG compression degraded the raw images, as apparent by the absence of the three

sets of six specks. For purposes of cancer detection, the images captured at lower doses

should be as unaltered as possible before they are processed in order to avoid the

aforementioned loss due to compression. The four images are portrayed in figures 12-15.

Figure 12 Low dose mammography image of the American College of Radiology (ACR) phantom captured 75 mRad. Evidence of low contrast, scattering, and noise degradation is apparent.
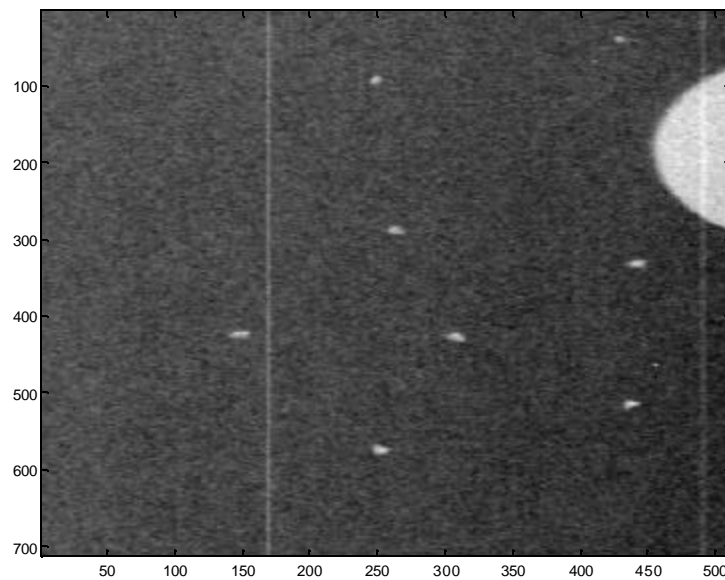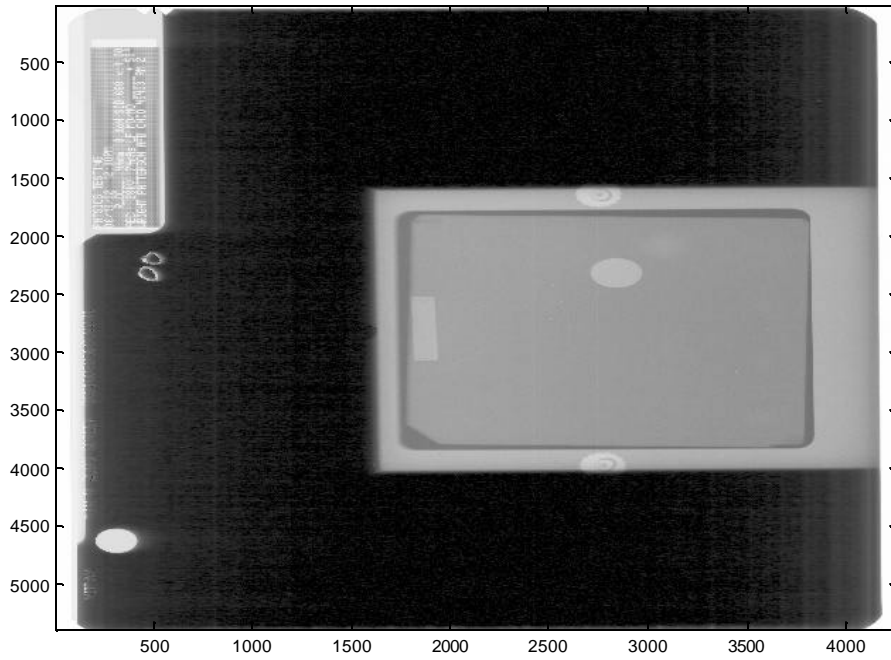
Figure 13 Low-medium dose mammography image of the American College of Radiology (ACR) phantom captured at 100 mRad. Evidence of low contrast, scattering, and noise degradation is still apparent.
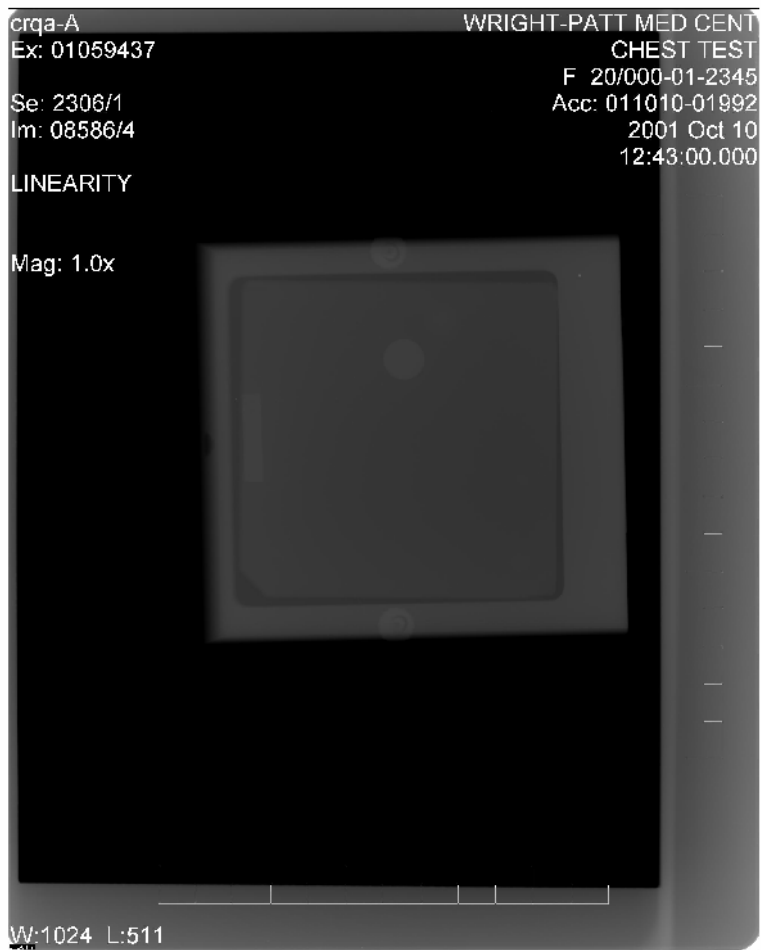
Figure 14 Medium-high dose mammography image of the American College of Radiology (ACR) phantom captured at 125 mRad. Evidence of low contrast, scattering, and noise degradation continues to be apparent.
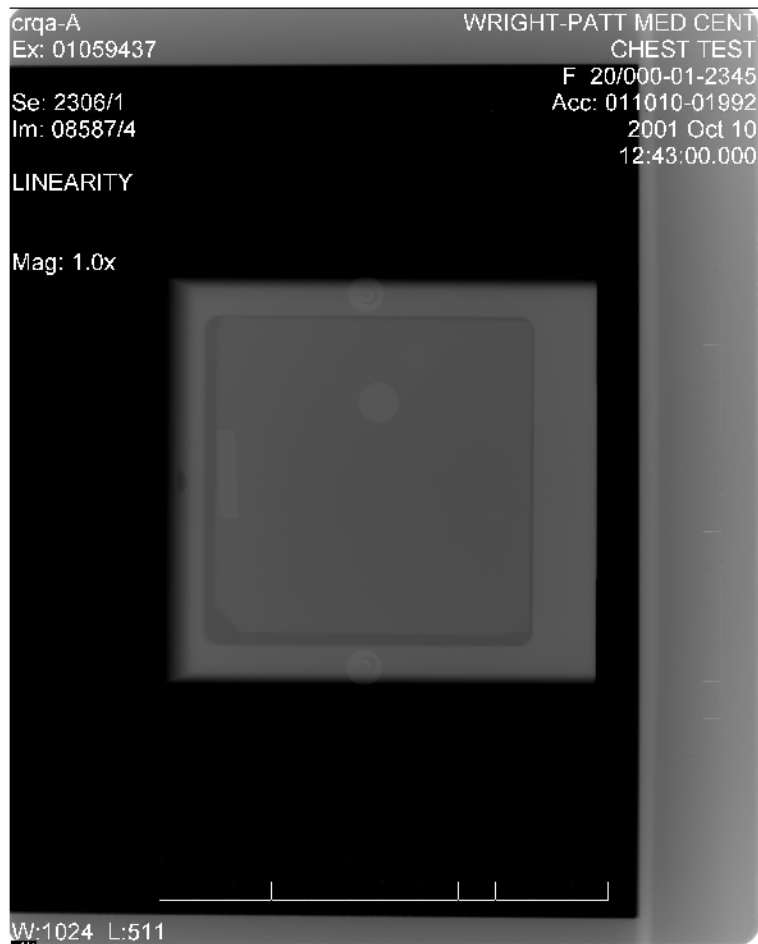
Figure 15 High dose mammography image of the American College of Radiology (ACR) phantom captured at 150 mRad.

The aforementioned procedure for obtaining images yielded images that were not useable due to the severe degradation in details. As a result, the following describes a more reliable procedure used to obtain the digitized images:

1) Use a Howtek MultiRAD 850 digitizer furnished by Qualia Computing, Inc., to scan the mammography images

2) Save the scanned images uncompressed

The procedure was used to obtain six images at varying doses: 1) 50 mRad, 2) 100 mRad, 3) 110 mRad, 4) 120 mRad, 5) 130 mRad, and 6) 150 mRad designated Very-low dose, Low dose, Low-medium dose, Medium-high dose, High dose, and Very-high dose respectively. The six images are shown in figures 16-27.
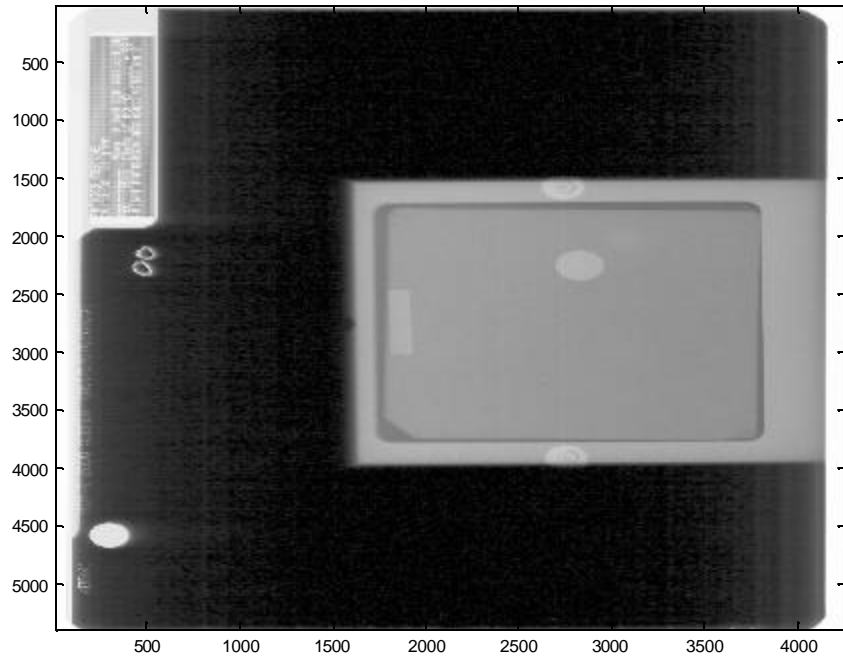
Figure 16 Very-low dose mammography image of the American College of Radiology (ACR) phantom captured 50 mRad. Evidence of low contrast, scattering, and noise degradation is apparent.
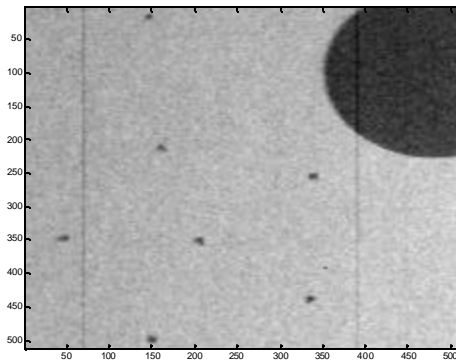
Figure 17 Zoomed in image of the complement of the Very-low dose (50 mRad) image with one set of specks and disk shown.
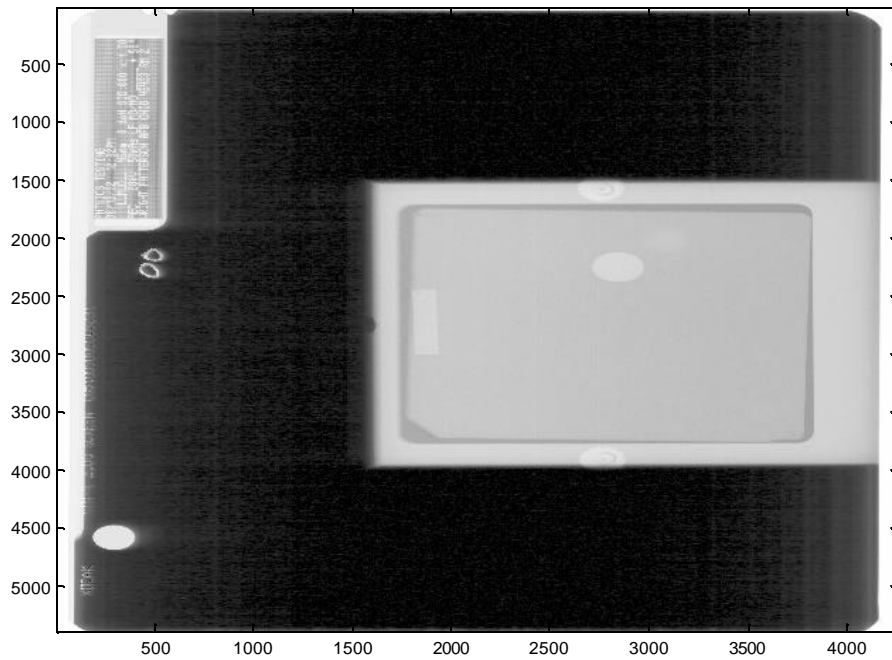
Figure 18 Low dose mammography image of the American College of Radiology (ACR) phantom captured 100 mRad. Evidence of low contrast, scattering, and noise degradation is apparent.
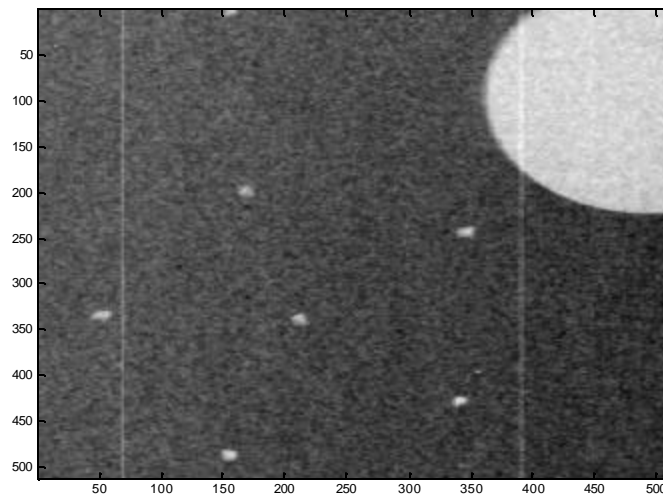
Figure 19 Zoomed in image of the Low dose (100 mRad) image with one set of specks and disk shown.
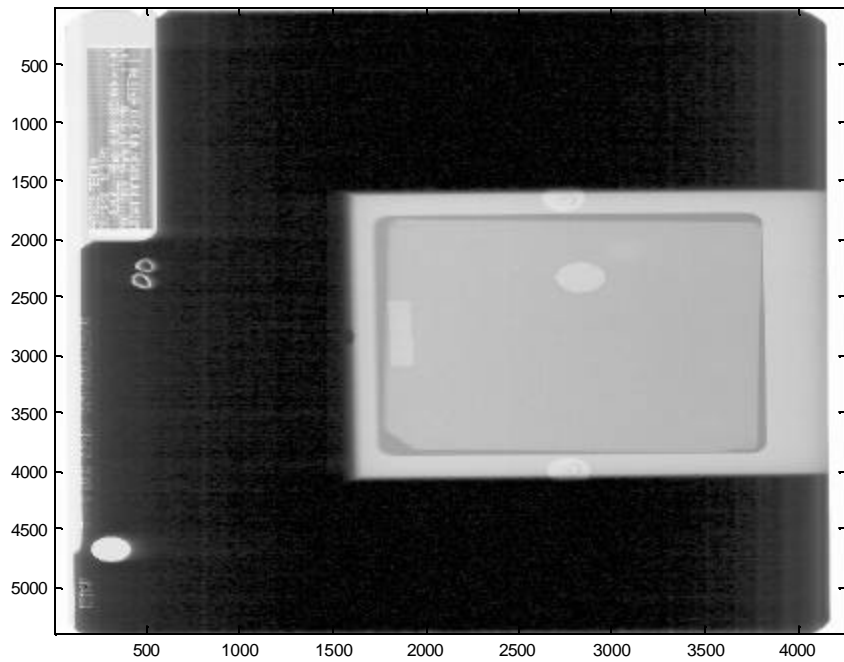
Figure 20 Low-medium dose mammography image of the American College of Radiology (ACR) phantom captured 110 mRad. Evidence of low contrast, scattering, and noise degradation is apparent
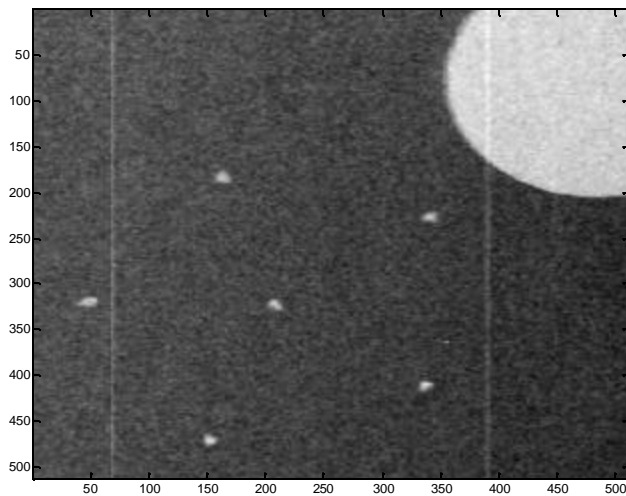
Figure 21 Zoomed in image of the Low-medium dose (110 mRad) image with one set of specks and disk shown.

34
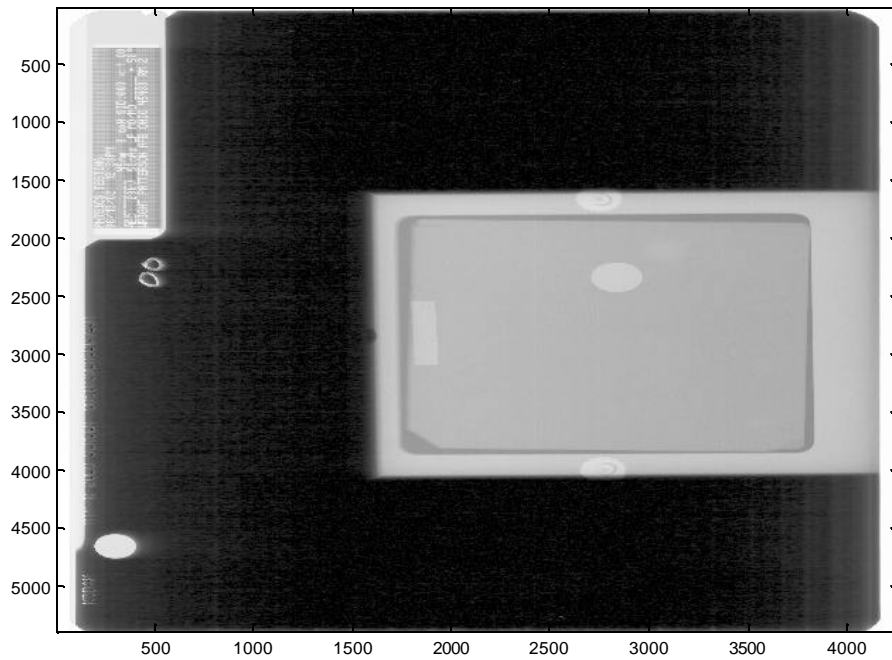
Figure 22 Medium-high dose mammography image of the American College of Radiology (ACR) phantom captured 120 mRad. Evidence of low contrast, scattering, and noise degradation is apparent.
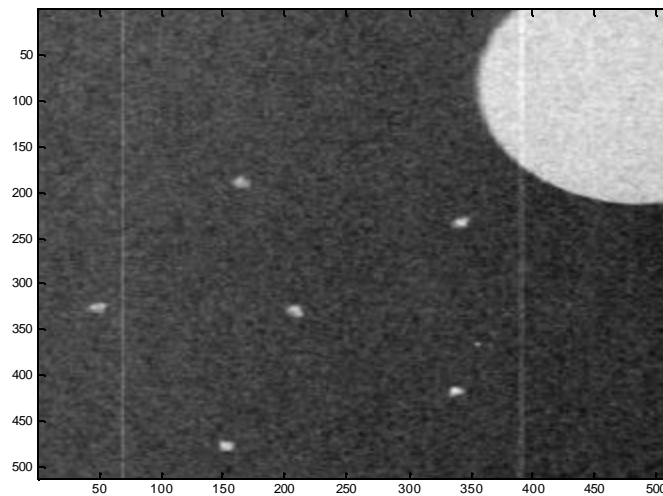
Figure 23 Zoomed in image of the Medium-high dose (120 mRad) image with one set of specks and disk shown.
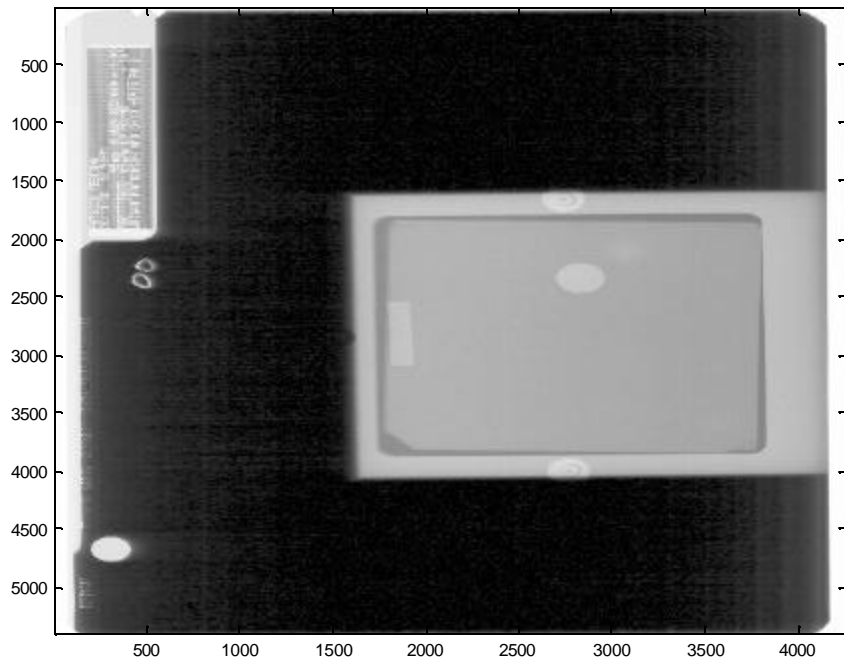
Figure 24 High dose mammography image of the American College of Radiology (ACR) phantom captured 130 mRad. Evidence of low contrast, scattering, and noise degradation is apparent.

Figure 25 Zoomed in image of the High dose (130 mRad) image with one set of specks and disk shown.

Figure 26 Very-high dose mammography image of the American College of Radiology (ACR) phantom captured 150 mRad. Evidence of low contrast, scattering, and noise degradation is apparent. This image represents the current standard for image quality and meets the radiologist requirement for mammography diagnosis.
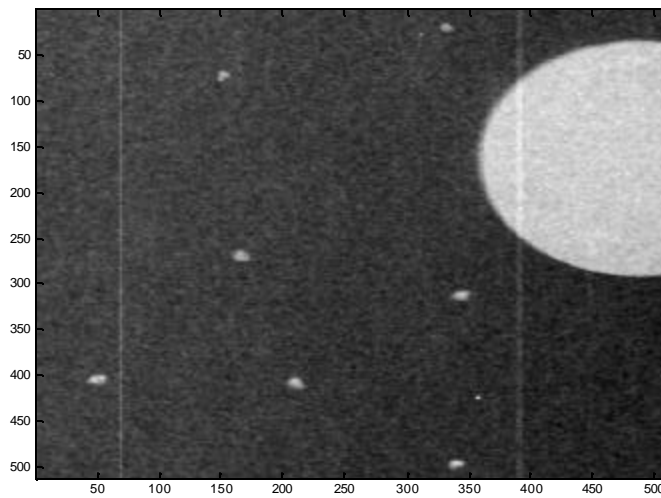
Figure 27 Zoomed in image of the Very-high dose (150 mRad) image with one set of specks and disk shown.

3.2 Procedure for processing the very-low dose image

The six images were imported into the MATLAB workspace and the following processing on the images was performed: 1) nonuniform illumination correction, 2) histogram equalization, 3) Wiener filtering, 4) RDWT denoising, and 5) edge detection.

One priority is to reduce the effects of X-ray scatter. X-ray scatter creates an uneven illumination in the mammography image, meaning that the image at the epicenter of the X-ray beam is brighter than the image towards the perimeter. In order to address this problem, an uneven illumination background correction was employed based on the unsharp masking principle of subtracting a lower resolution image from the original image to obtain only the higher resolution portion. The following procedure was executed:

1) The 5400 x 4262 pixel image is partitioned into 200 x 200 blocks.

2) The minimum of each block is determined to create a coarse estimate of the background.

3)   The coarse estimate is subtracted from the histogram equalized image

The image was partitioned into 200 x 200 blocks after experimentation with various partition sizes. When smaller partition sizes were used, objects of interest were lost. As a result, the block sizes were chosen to be greater than the largest object of interest which was the disk in the ACR phantom. Partition sizes greater than the 200 x 200 blocks did not reduce the nonuniform background as well. This method is advantageous when a priori information of the image is present. In this case, the size of the disk and microcalcifications were known, making the choice of the 200 x 200 partition size practical. In mammography images with actual breast specimens, the nonuniform

correction would be replaced with a more traditional unsharp masking method that would subtract a low-pass filtered image from the original image. Figure 28 shows the coarse estimate of the uneven illumination background of the low dose image followed by Figure 29, which shows the spatial representation of the coarse estimate.
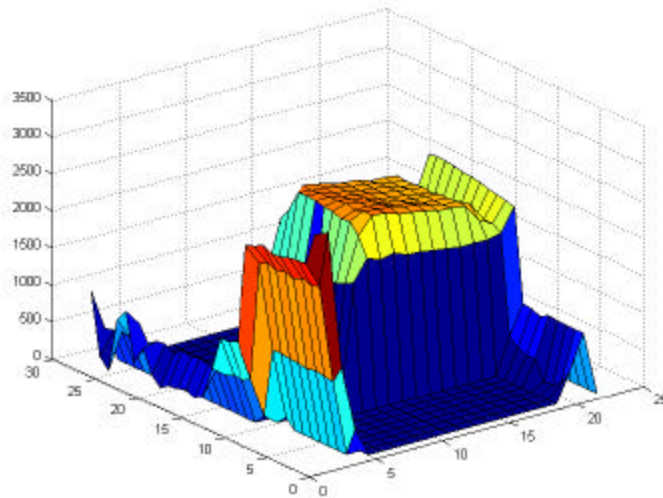
Figure 28 Coarse estimate of the very-low dose (50 mRad) image found by creating a background consisting of 200 x 200 blocks with vertices corresponding to the minima of the 200 x 200 blocks of the original image
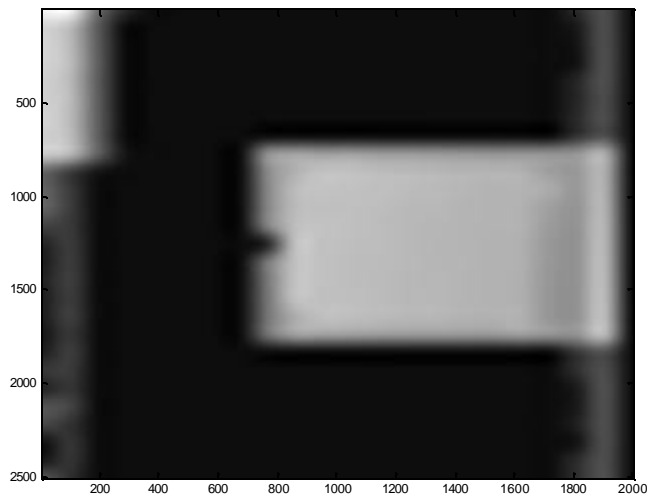
Figure 29 Spatial representation of the coarse estimate of the very-low dose (50 mRad) image background

The coarse estimate of the low dose mammography image background is then subtracted

from the histogram equalized image to obtain the image of Figure 30.
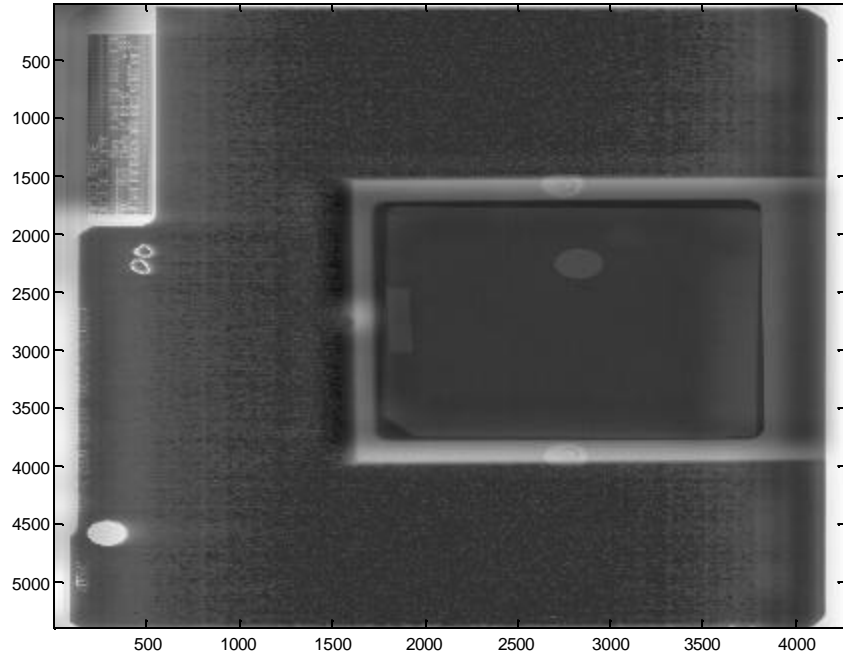
Figure 30 Uneven illumination corrected very-low dose (50 mRad) image.

Another priority is to improve the contrast of the images. Figure 31 shows the

histogram of the raw very-low dose image.
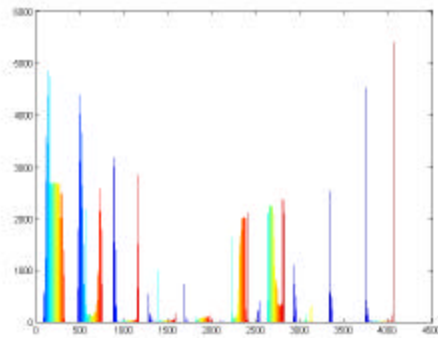
Figure 31 Histogram of very-low dose (50 mRad) image.

This histogram shows that the pixels of the very-low dose image are predominantly dark since most of the pixels have lower grayscale values (The grayscale spectrum ranges from 0 for black to 255 for white). The histogram of the very-low dose image also shows that the image has low contrast, since the histogram is "peaky" and not spread out uniformly as in the case of high contrast images. Figure 32 shows the uneven illumination corrected, histogram equalized very-low dose image.
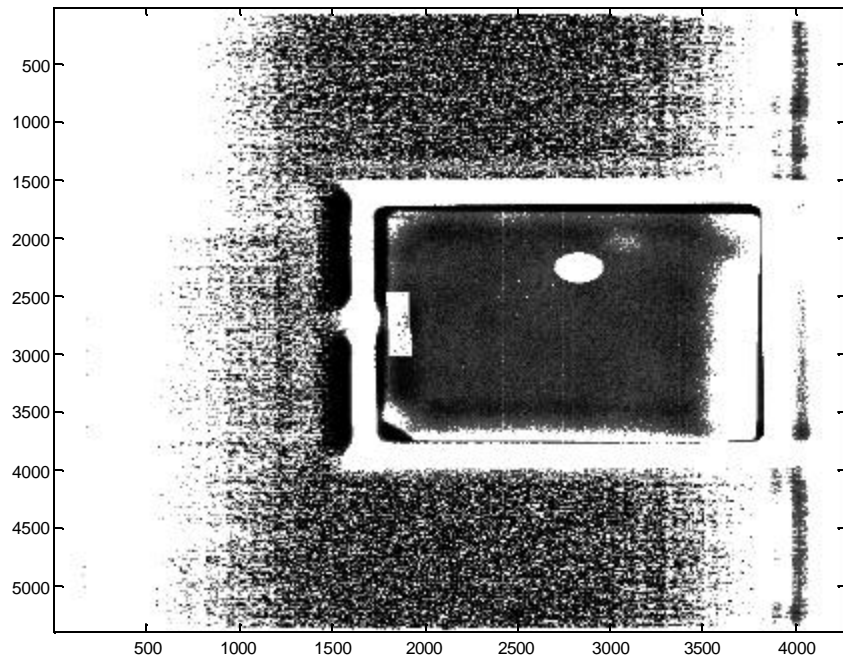
Figure 32 Uneven illumination corrected, histogram equalized very-low dose (50 mRad) image.

Histogram equalization was performed using the MATLAB function HISTEQ. The ACR phantom is more distinguishable after histogram equalization. To explain this phenomenon, a histogram of the histogram equalized image is shown Figure 33.
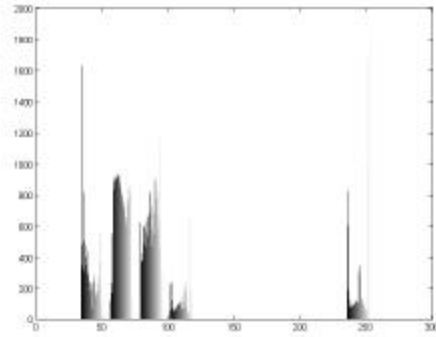
Figure 33 Histogram of uneven illumination corrected, histogram equalized very-low dose (50 mRad) image.

The histogram of the uneven illumination corrected, histogram equalized very-low dose image is more uniform then the histogram of the very-low dose image. By multiplying the pixels corresponding to the "peaky" portion of the histogram of the low dose image by a high slope, an image with improved contrast is obtained. This aids in a very important priority for improving mammography, contrast enhancement.

The third priority in improving breast imaging is noise reduction. In order to reduce Gaussian noise, the Wiener filter was applied. Using the MATLAB function WIENER2, 2-D adaptive noise removal filtering on the uneven illumination corrected, histogram equalized low dose image was performed. The signal dependant scatter effects were treated as a blurring effect. As a result, the adaptive Wiener filter with deblurring was chosen to counter the effects of the blurring resulting from scatter noise. The other denoising filter investigated was the median filter. The median filter was not practical for the research at hand due to its eradication of minute objects such as microcalfications. The median filter also does not counter blur caused by the scatter noise. Based on statistics from the local area of each pixel, the adaptive Wiener filter denoised the image

42

to yield the uneven illumination corrected, histogram equalized, Wiener denoised very-low dose image shown in figure 34.
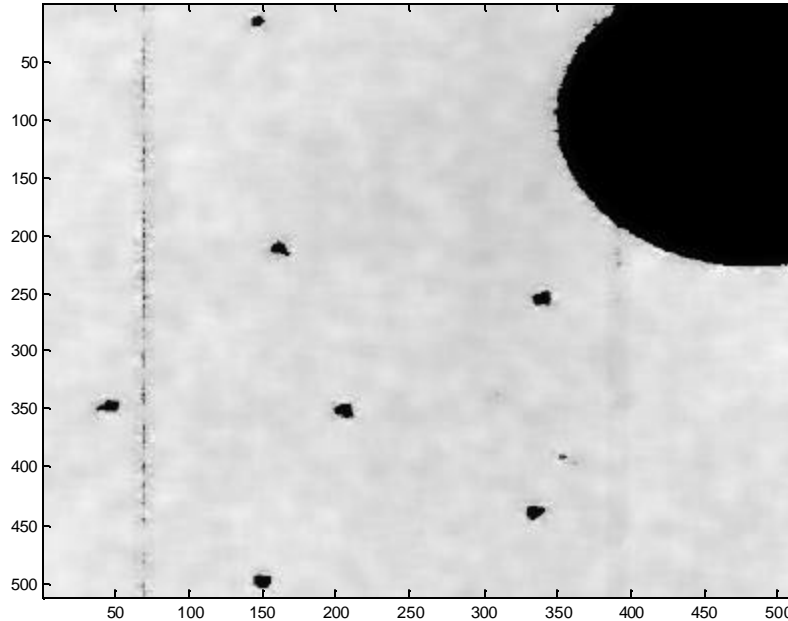
Figure 34 Uneven illumination corrected, histogram equalized, Wiener denoised very-low dose (50 mRad) image. The uneven illumination correction subtracts a coarse estimate of the non-uniform background, giving the low dose image a more uniform background. The histogram equalization makes the histogram of the low dose image more uniform, which equates to higher contrast. The Wiener filter provides an adaptive denoising method to reduce the Gaussian noise present at low doses.

The Wiener filtered image eradicated the noise in the image, however, the background is

blotchy. Artifacts at the edges of the disk and specks is apparent due to the adaptive filter

taking into account the high contrast change between the background and the disk and

specks.

As a substitute to the Wiener denoising, the RDWT denoising was employed.

The combined effects of denoising and enhancement that the RDWT denoising system

provides made it advantageous to the research at hand. Figure 35 shows the uneven
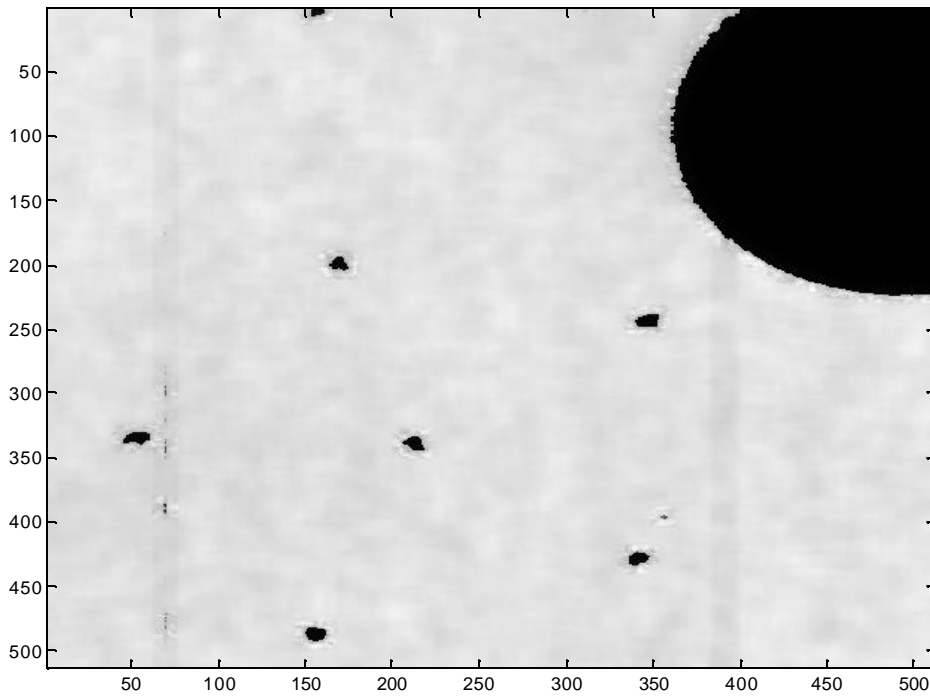
illumination corrected, histogram equalized, RDWT denoised very-low image.
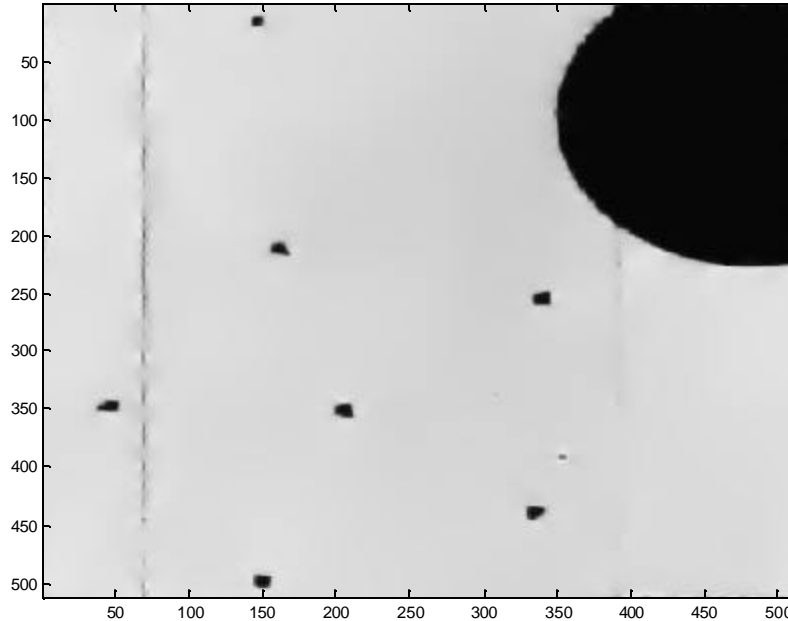
Figure 35 uneven illumination corrected, histogram equalized, RDWT denoised very-low dose (50 mRad) image.

The RDWT denoised image has a smooth background and very little artifacts at the edges

of the disk and specks. An appearance of bleeding is apparent at the edges of the disk

and the specks but is not significant enough to cause misdiagnosis. The RDWT

denoising scheme was chosen over the Wiener filtering since the Wiener filtering caused

more artifacts and the background contrast was not as uniform.

In order to aid in detecting the microcalcifications and masses in the image, edge

detection methods were analyzed. The MATLAB function EDGE was implemented

using two methods: Canny and Prewitt. Figure 36 shows the edge-detected post-

processed low dose mammography image using the Canny method.
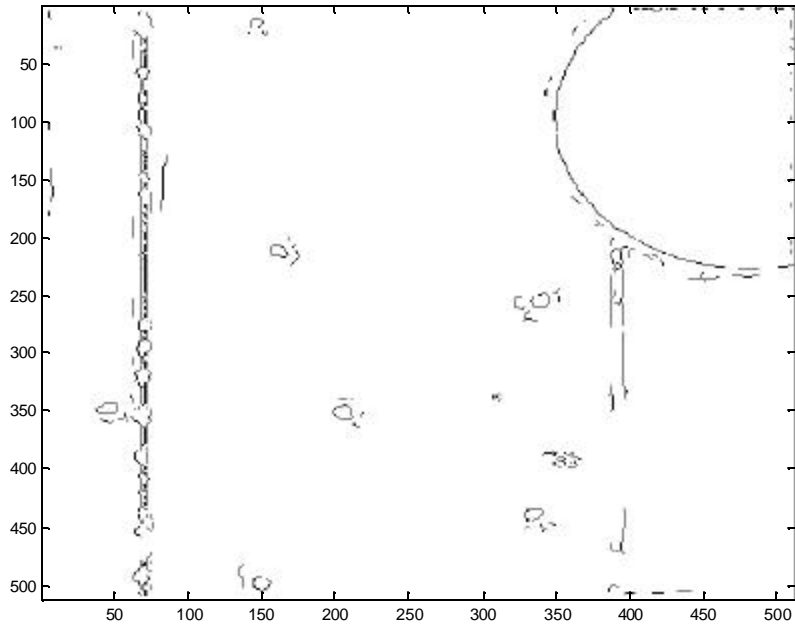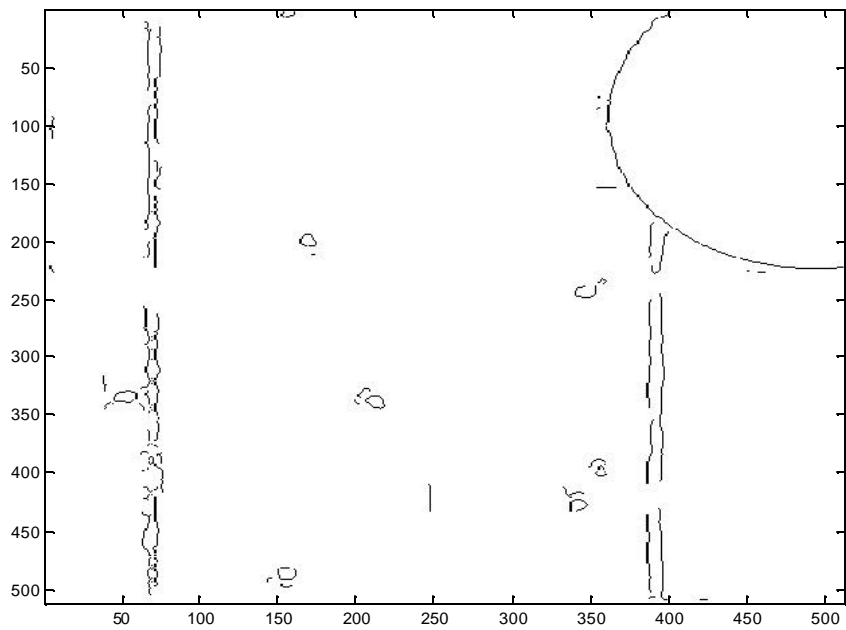
Figure 36 Edge detected post-processed very-low dose (50 mRad) image using the Canny method.
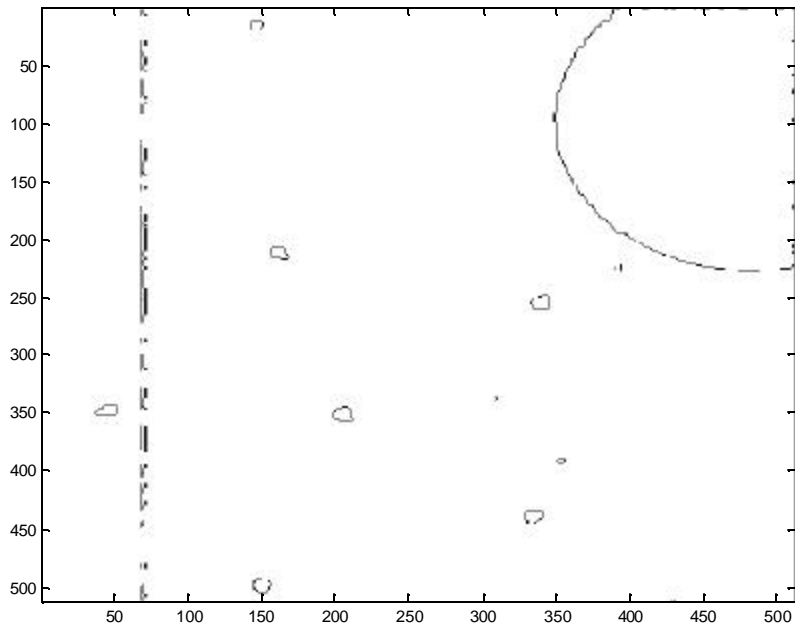
Figure 37 Edge detected post-processed very-low dose (50 mRad) image using the Prewitt method. The Prewitt method utilizes a gradient operator, which measures the gradient of the image to determine where edges occur.

The Canny method of edge detection has two thresholds, one for weak edges and one for prominent edges. The weak edges that are connected to the prominent edges are considered edges in the Canny method. The Prewitt method does not take into consideration the weak edges. The Prewitt edge detection method brings out just enough detail to detect the objects of interest. As a result, the Prewitt edge detection method is more beneficial to the research at hand in detecting only the microcalcifications and the disk.

3.3 Procedure for processing low, low-medium, medium-high, and high dose images

The process of uneven illumination correction, histogram equalization, Wiener denoising, RDWT denoising and edge detection using the Canny and Prewitt methods was repeated for the low, low-medium, medium-high, and high dose images. Figures 38 through 77 represent the results of each phase of the processing for the two images.

3.3.1 Processing of the Low dose image
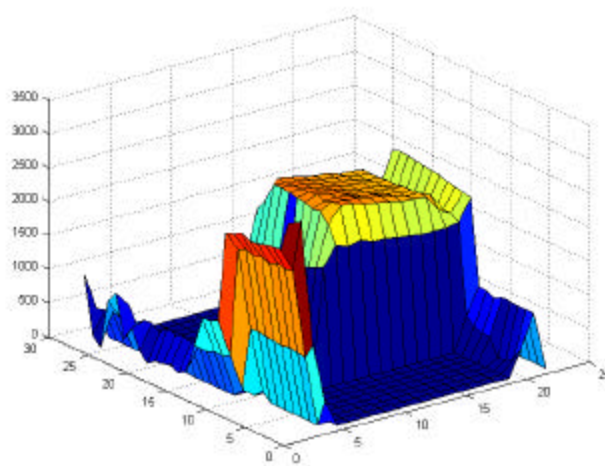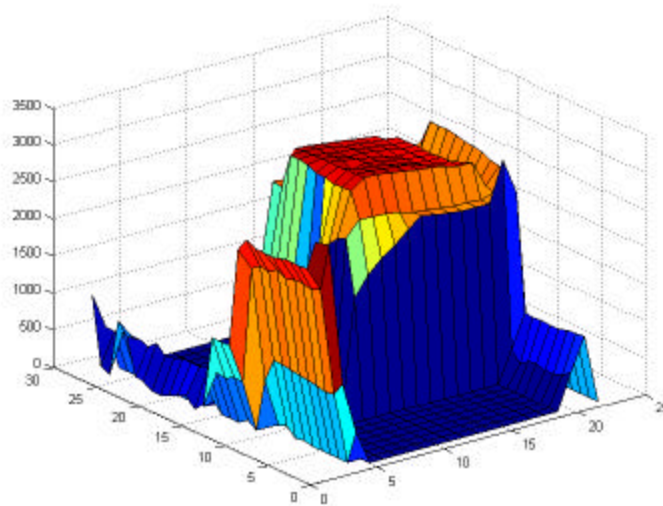

Figure 38 Coarse estimate of the Low dose (100 mRad) image.
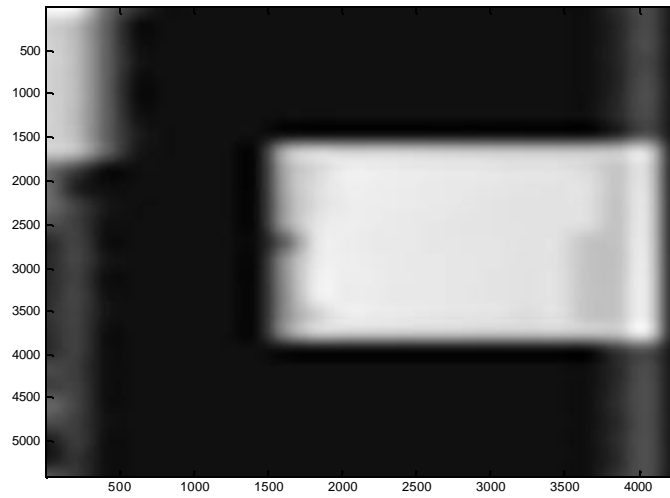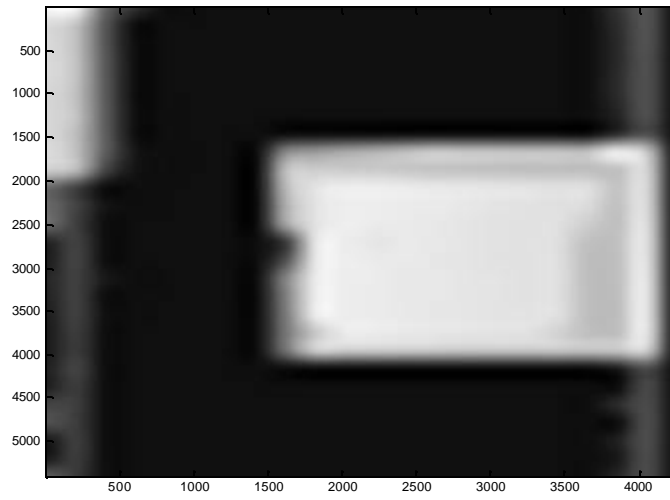
Figure 39 Spatial representation of the coarse estimate of the Low dose (100 mRad) image background.
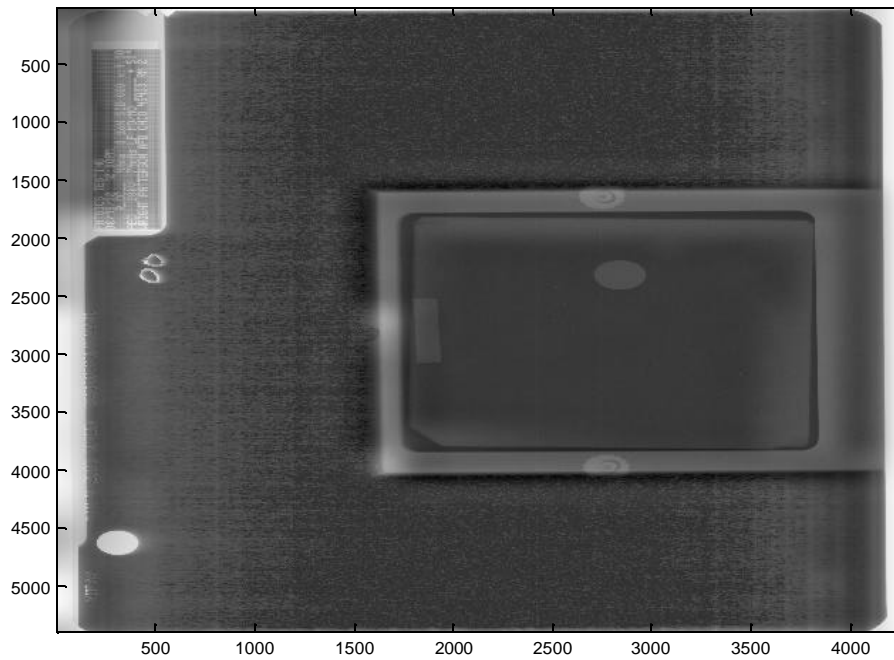
Figure 40 Uneven illumination corrected Low dose (100 mRad) image.
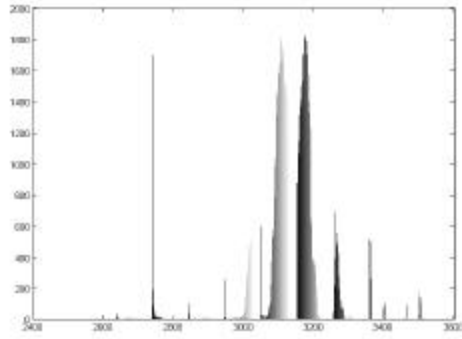
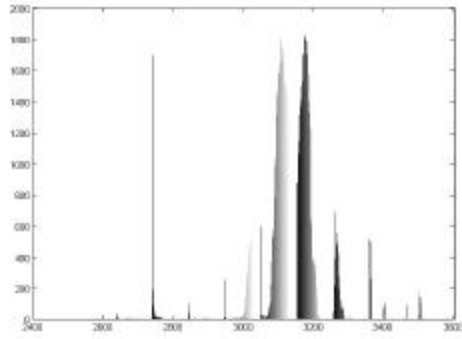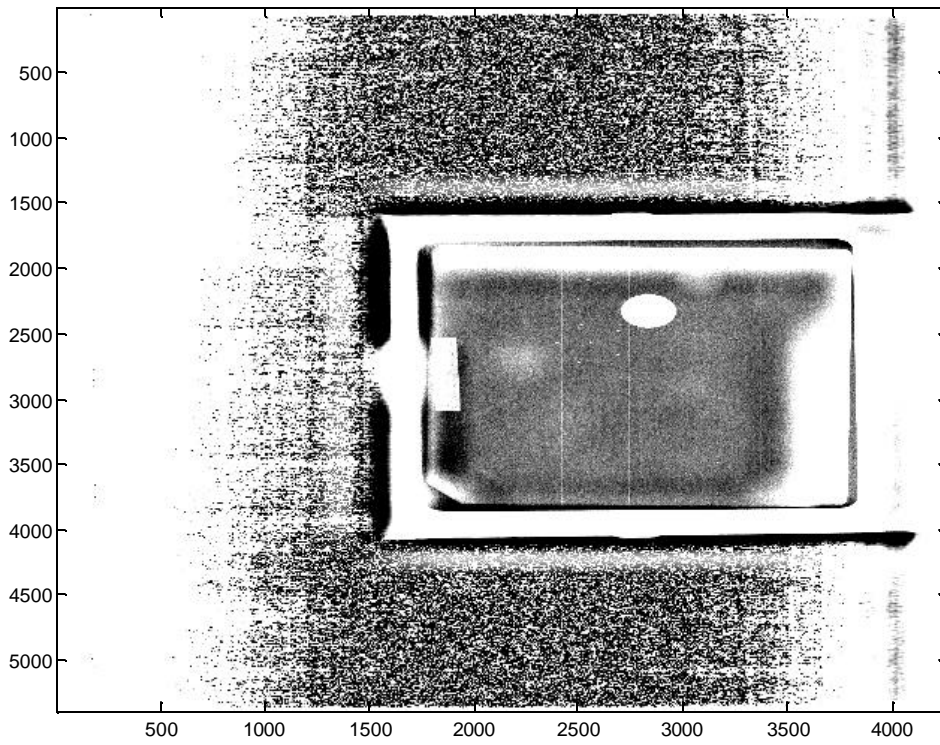Figure 41 Histogram of the Low dose (100 mRad) image.
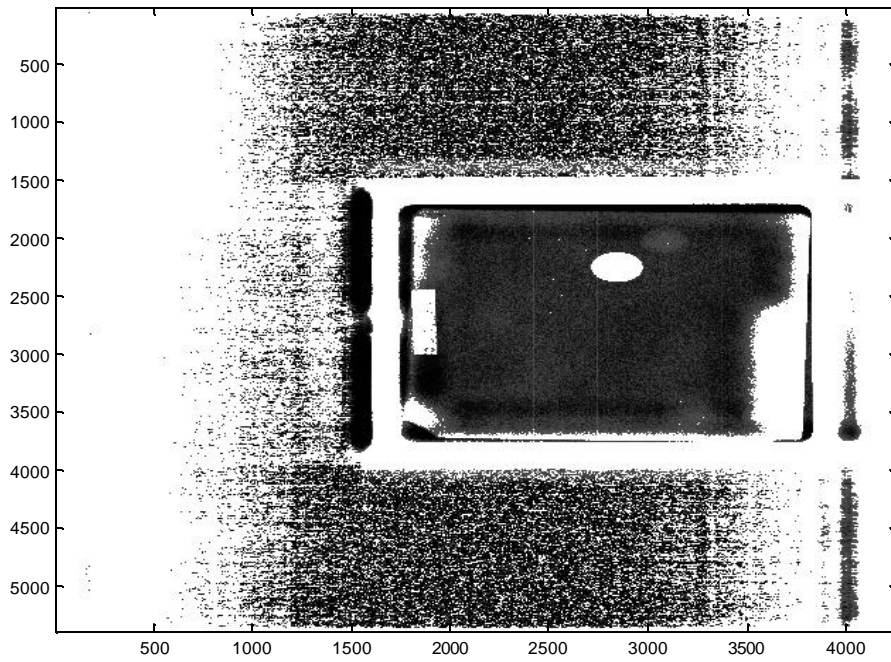
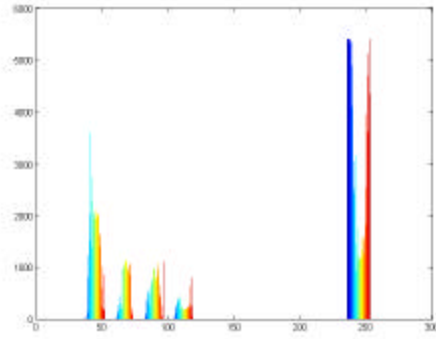Figure 42 Uneven illumination corrected, histogram equalized Low dose (100 mRad) image.

48
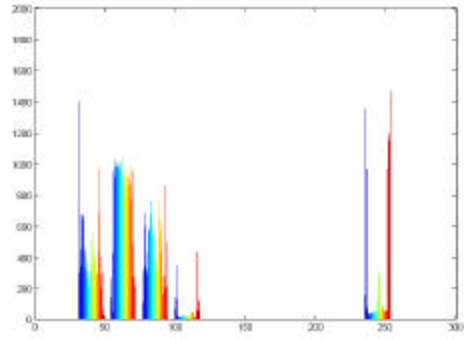
Figure 43 Histogram of the uneven illumination corrected, histogram equalized Low dose (100 mRad) image.

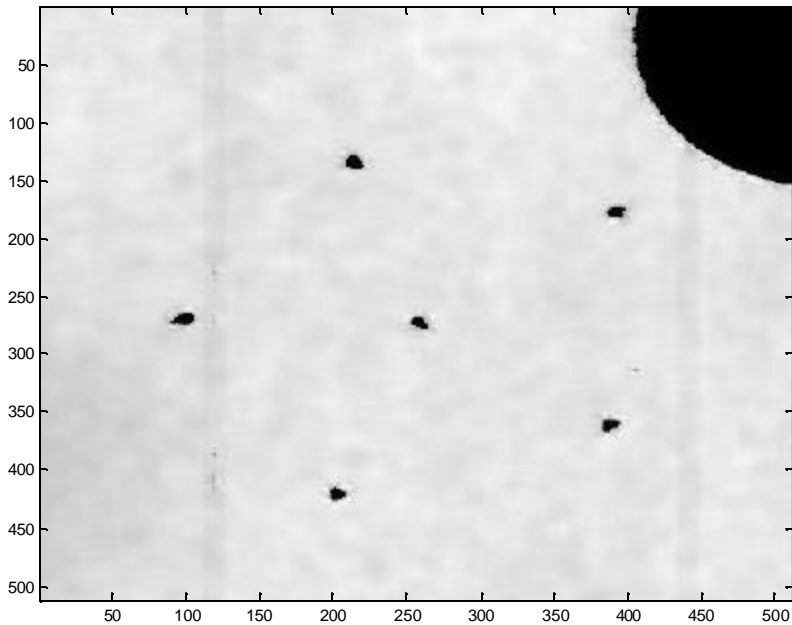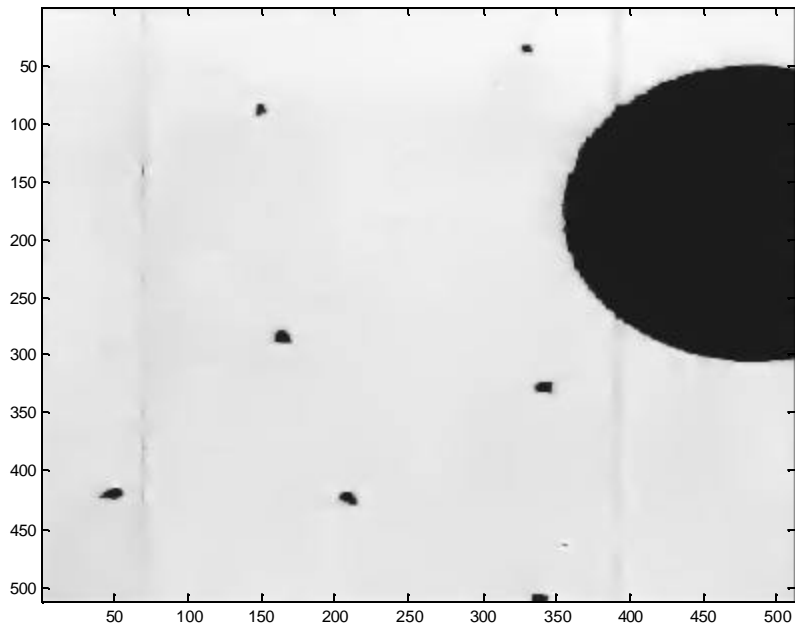Figure 44 Uneven illumination corrected, histogram equalized, Wiener denoised Low dose (100 mRad) image.
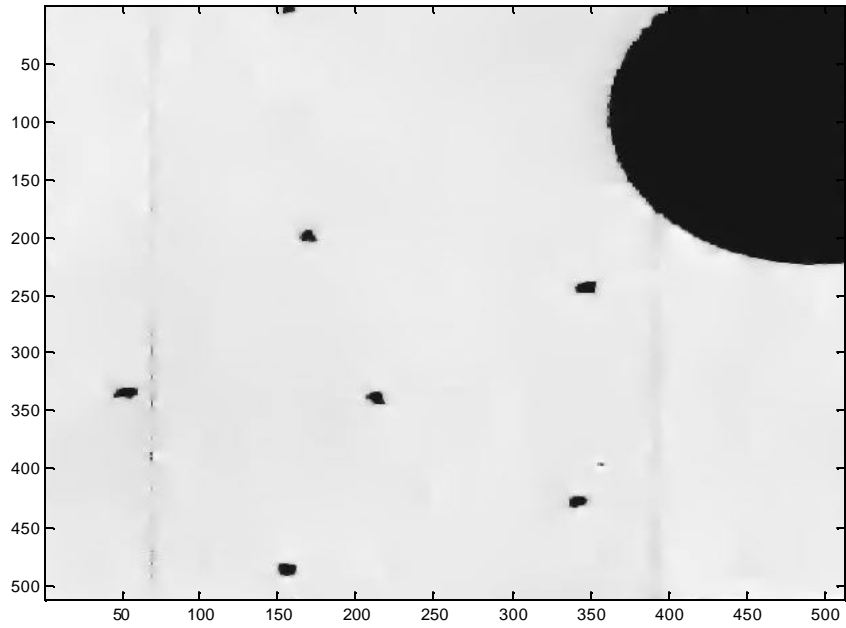
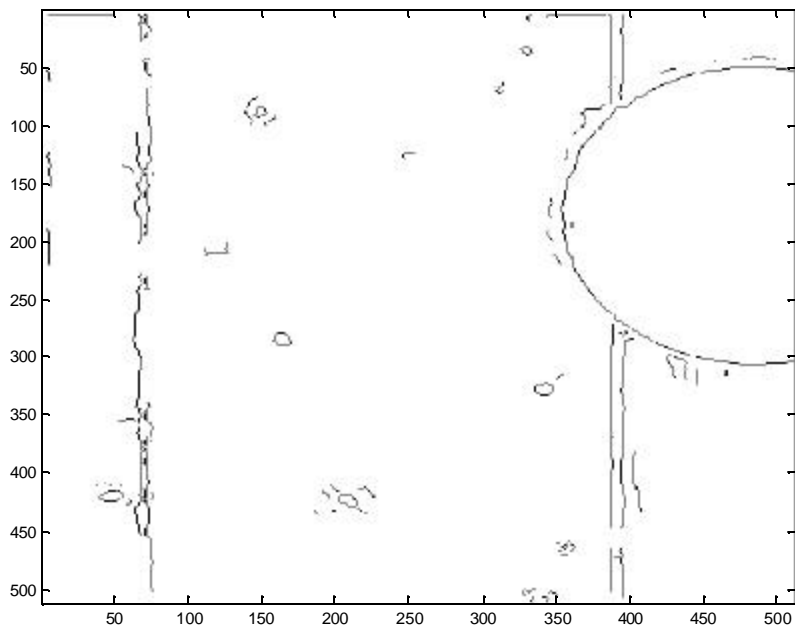Figure 45 Uneven illumination corrected, histogram equalized, RDWT denoised Low dose (100 mRad) image.

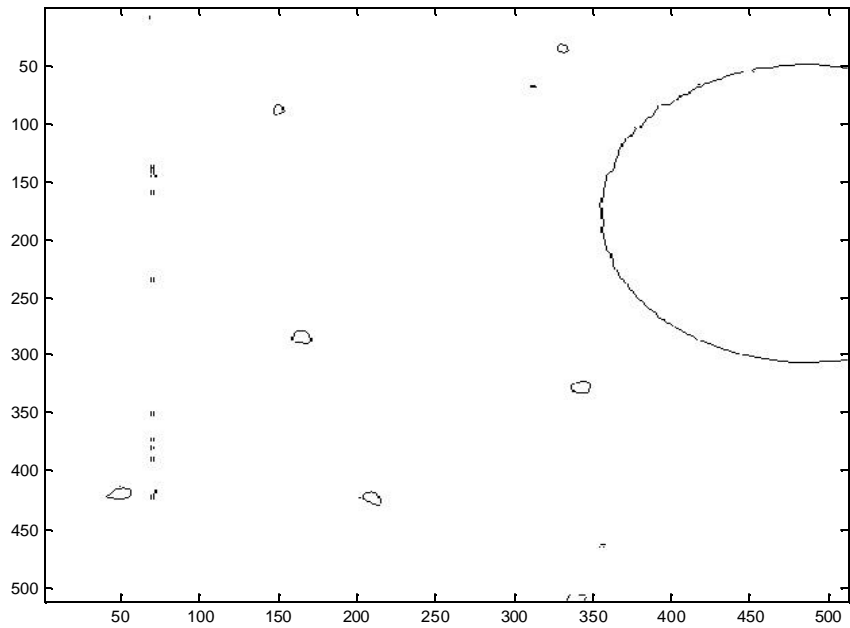Figure 46 Edge detected post-processed Low dose (100 mRad) image using the Canny method.
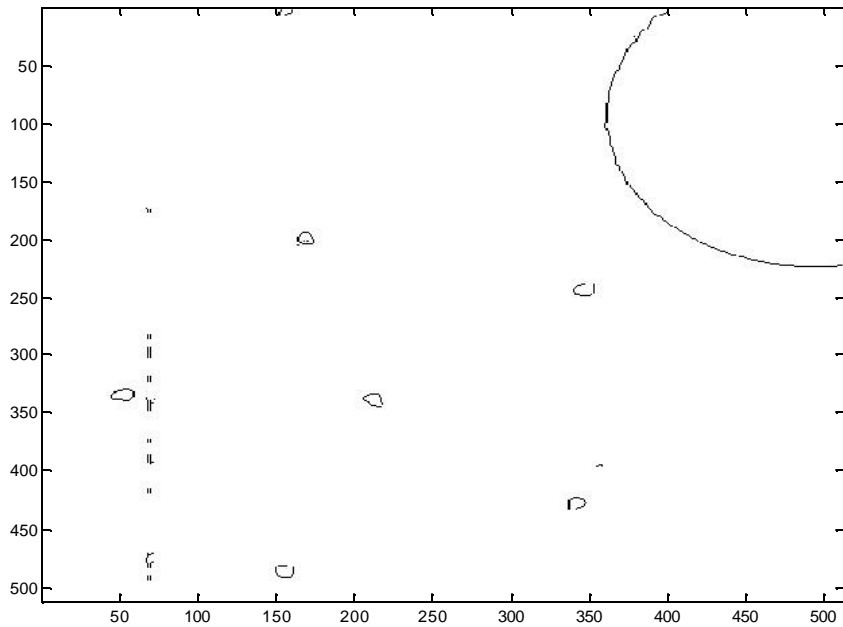
Figure 47 Edge detected post-processed Low dose (100 mRad) image using the Canny method.

3.3.2 Processing of the Low-medium dose image

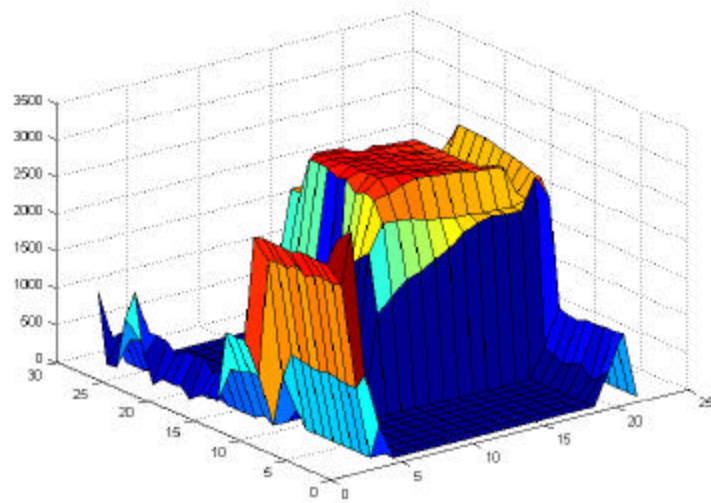Figure 48 Coarse estimate of the Low-medium dose (110 mRad).

Figure 49 Spatial representation of the coarse estimate of the Low-medium dose (110 mRad) image background.
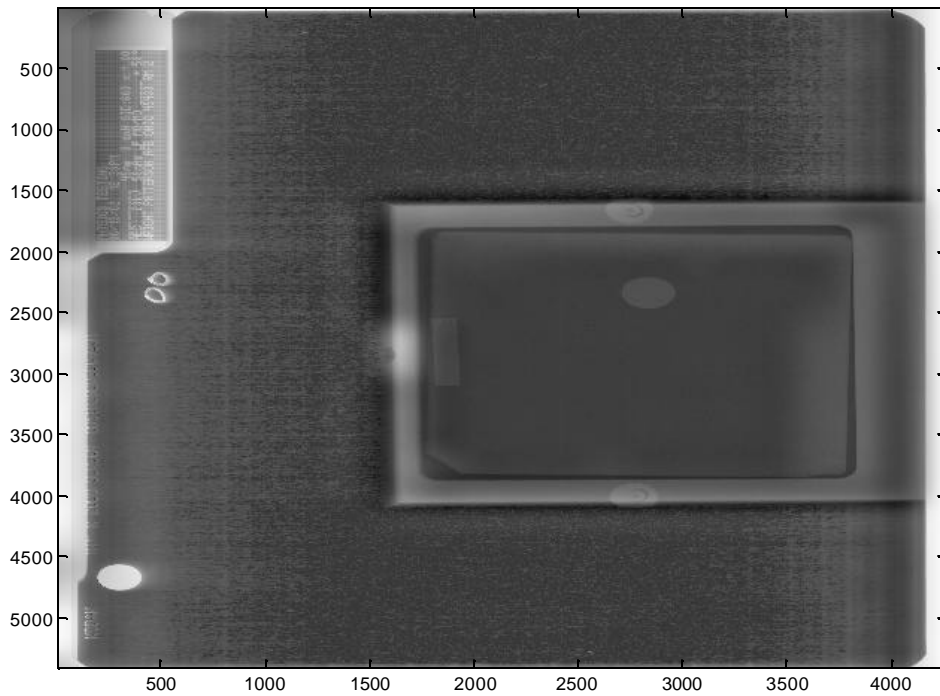
Figure 50 Uneven illumination corrected Low-medium dose (110 mRad) image.

Figure 51 Histogram of Low- medium dose (110 mRad) image.

Figure 52 Uneven illumination corrected, histogram equalized Low- medium dose (110 mRad) image.

Figure 53 Histogram of uneven illumination corrected, histogram equalized Low-medium dose (110 mRad) image.

Figure 54 Uneven illumination corrected, histogram equalized, Wiener denoised Low-medium dose (110 mRad) image.

Figure 55 Uneven illumination corrected, histogram equalized, RDWT denoised Low-medium dose (110 mRad) image.

Figure 56 Edge detected post-processed Low-medium (110 mRad) image using the Canny method.

Figure 57 Edge detected post-processed Low-medium (110 mRad) image using the Canny method.

3.3.3 Processing of the Medium-high dose image

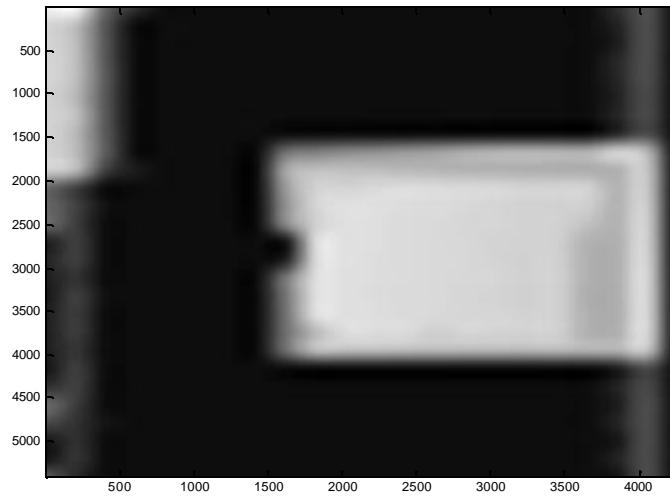Figure 58 Coarse estimate of the Medium-high dose (120 mRad) image.

Figure 59 Spatial representation of the coarse estimate of the Medium-high dose (120 mRad) image background.
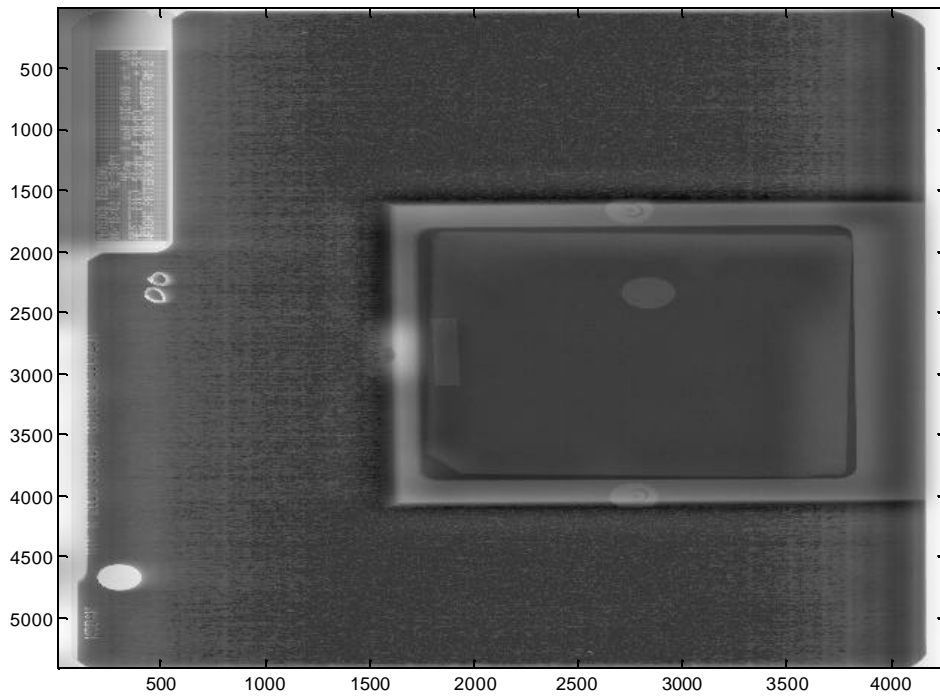

Figure 60 Uneven illumination corrected Medium-high dose (120 mRad) image.
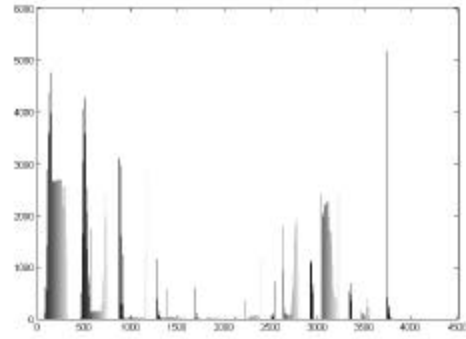
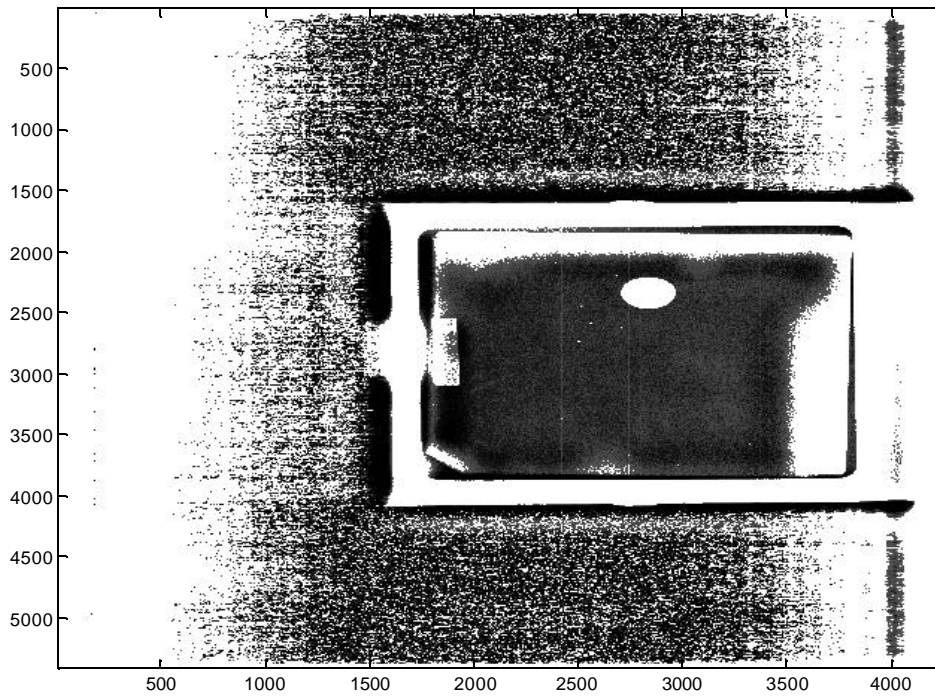Figure 61 Histogram of the Medium-high dose (120 mRad) image.

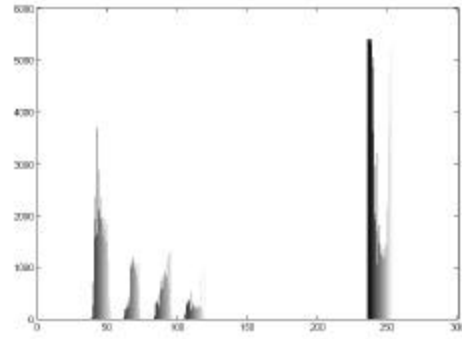Figure 62 Uneven illumination corrected, histogram equalized Medium-high dose (120 mRad) image.

Figure 63 Histogram of the uneven illumination corrected, histogram equalized Medium-high dose (120 mRad) image.
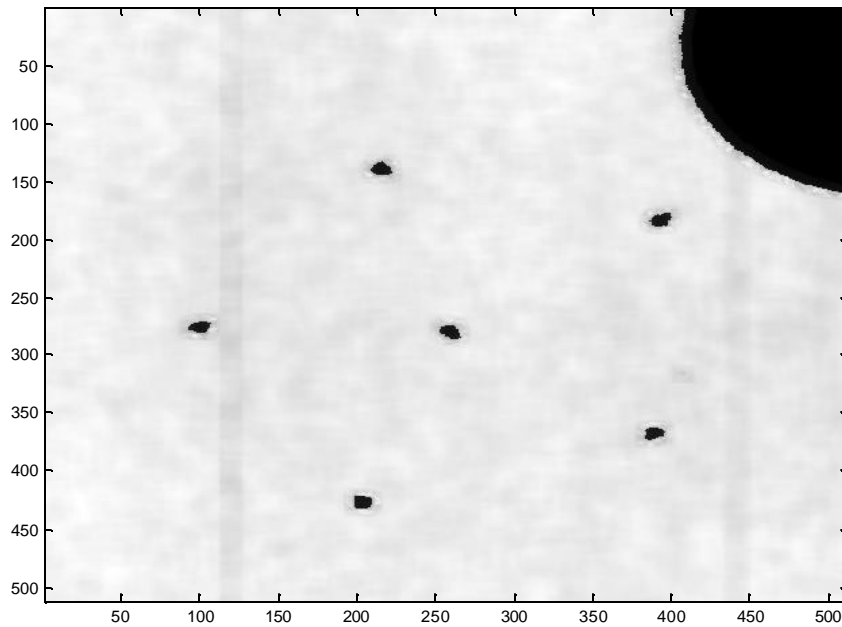

Figure 64 Uneven illumination corrected, histogram equalized, Wiener denoised Medium-high dose (120 mRad) image.
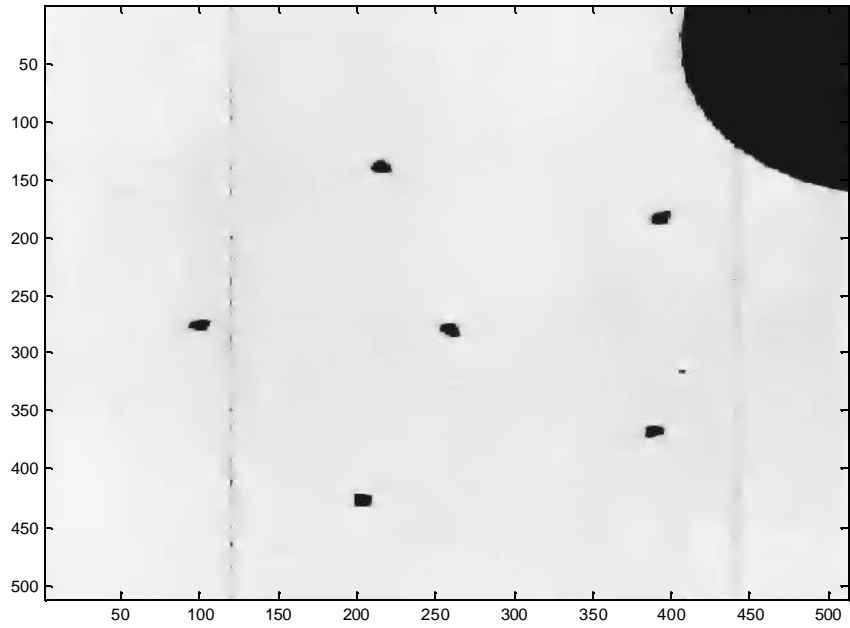
Figure 65 Uneven illumination corrected, histogram equalized, RDWT denoised
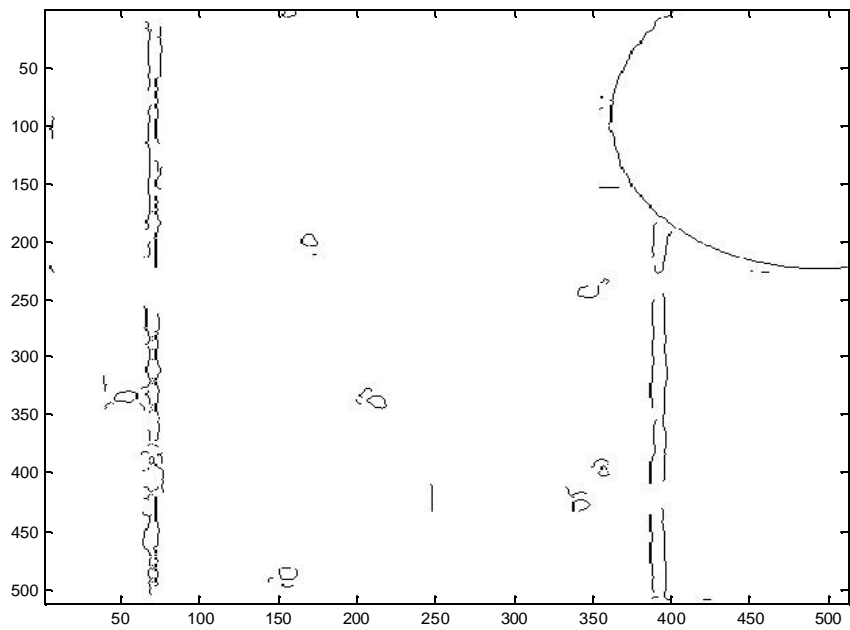Medium-high dose (120 mRad) image.

Figure 66 Edge detected post-processed Medium-high dose (120 mRad) image using the
Canny method.
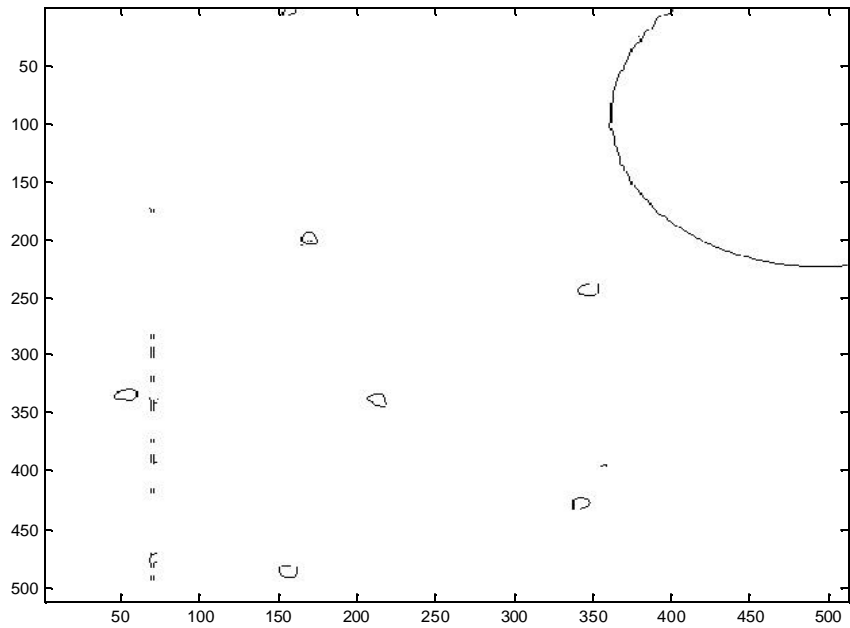
Figure 67 Edge detected post-processed Medium-high dose (120 mRad) image using the Prewitt method.

3.3.4 Processing of the High dose image
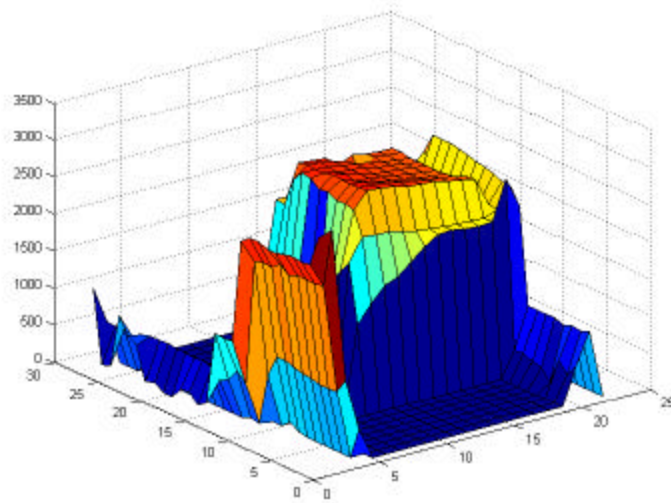

Figure 68 Coarse estimate of the High dose (130 mRad) image.
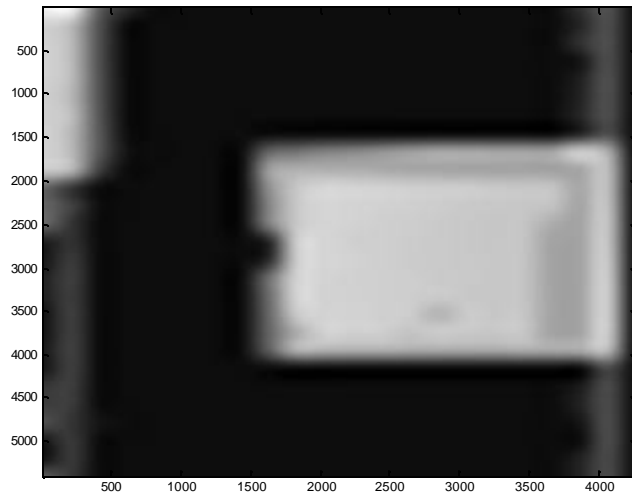
Figure 69 Spatial representation of the coarse estimate of the High dose (130 mRad) image.
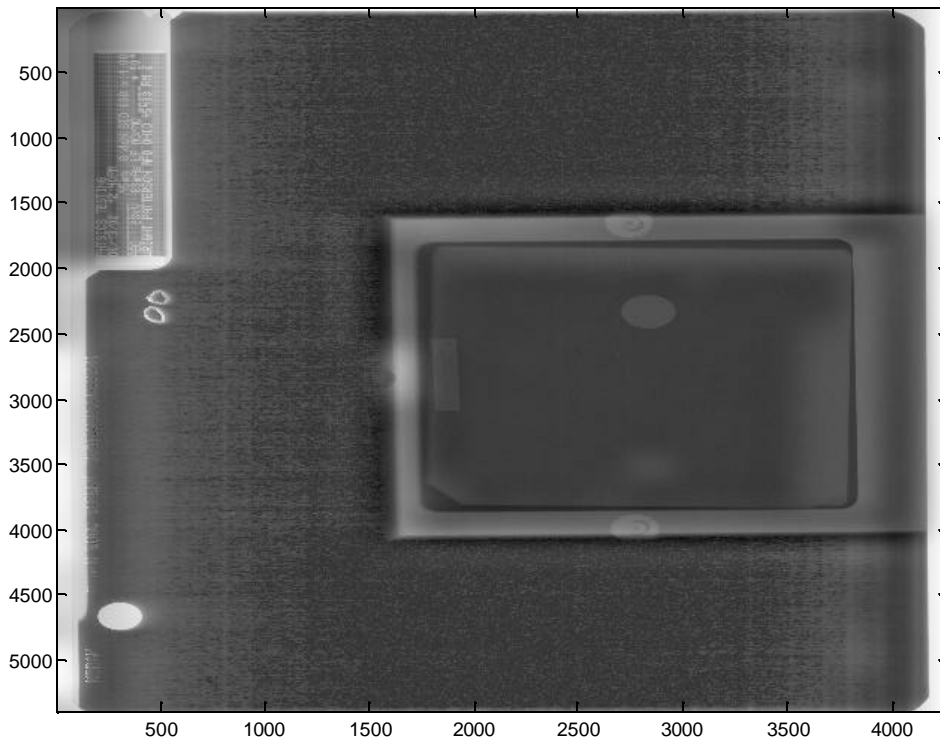
Figure 70 Uneven illumination corrected High dose (130 mRad) image.

Figure 71 Histogram of High dose (130 mRad) image.

Figure 72 Uneven illumination corrected, histogram equalized High dose (130 mRad) image.

Figure 73 Histogram of the uneven illumination corrected histogram equalized High dose (130 mRad) image.

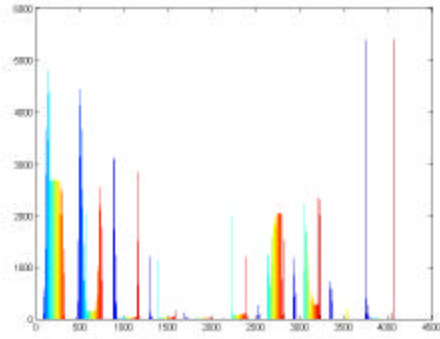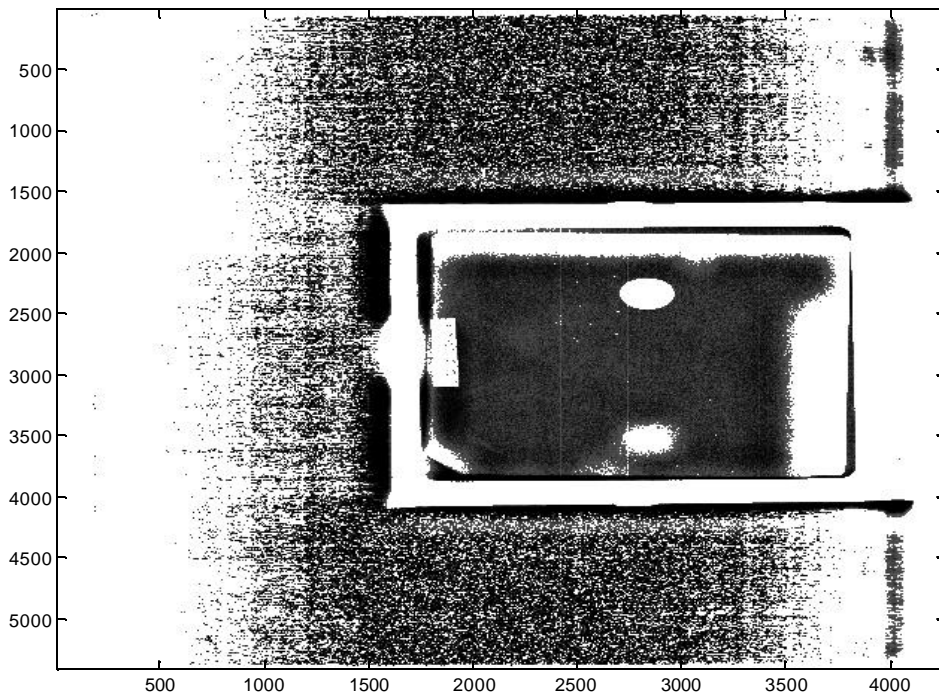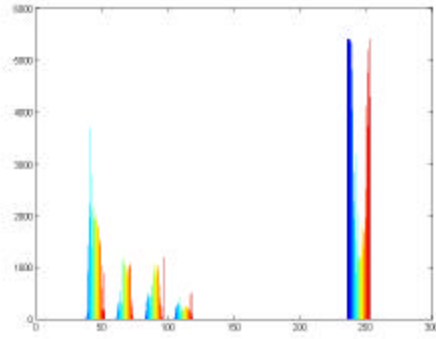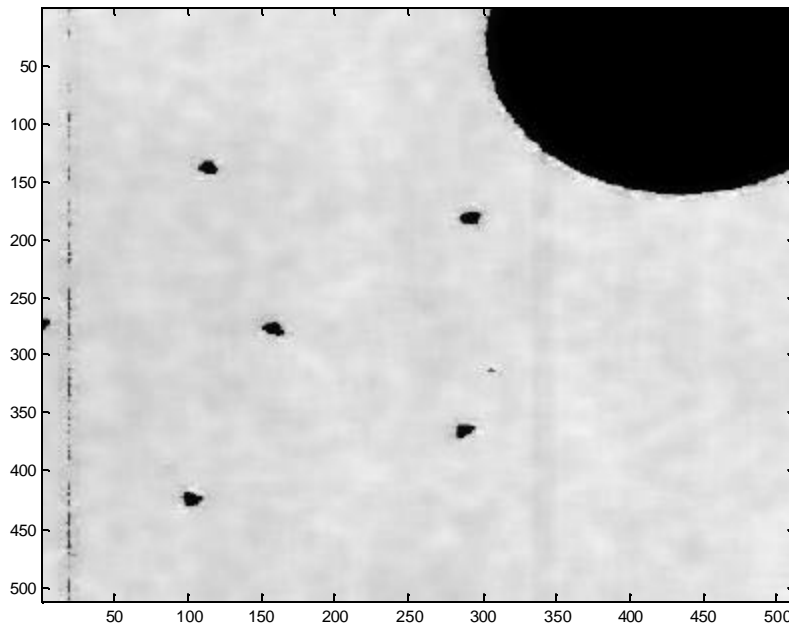Figure 74 Uneven illumination corrected, histogram equalized, Wiener denoised High dose (130 mRad) image.
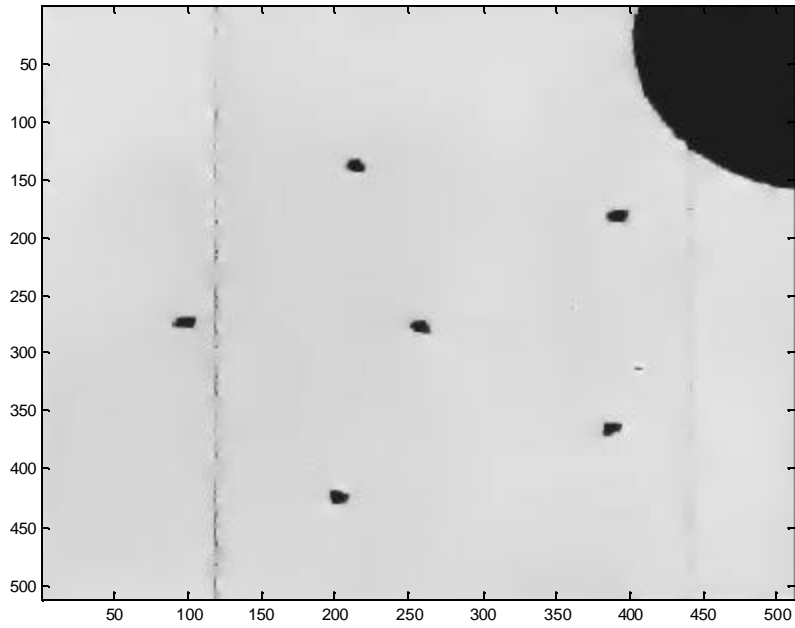
Figure 75 Uneven illumination corrected, histogram equalized, RDWT denoised High dose (130 mRad) image.
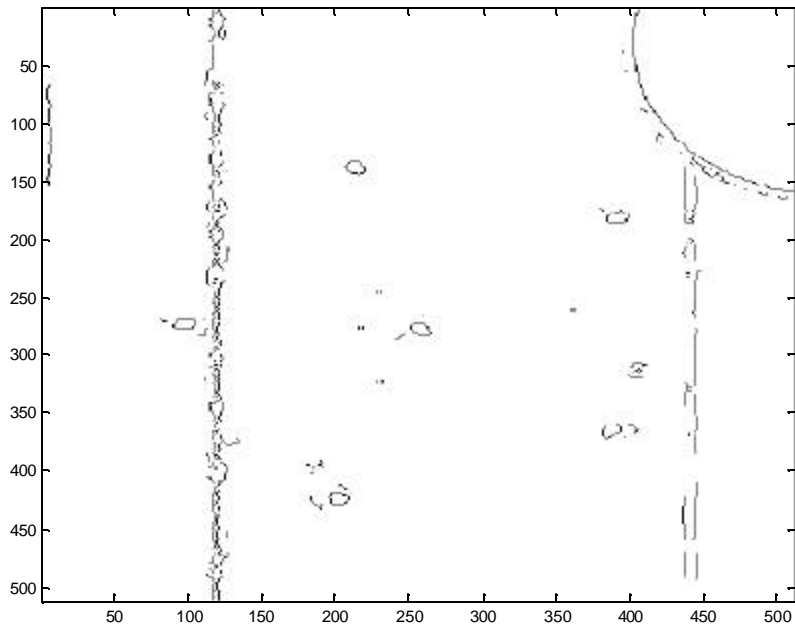
Figure 76 Edge detected post-processed High dose (130 mRad) image using the Canny method.
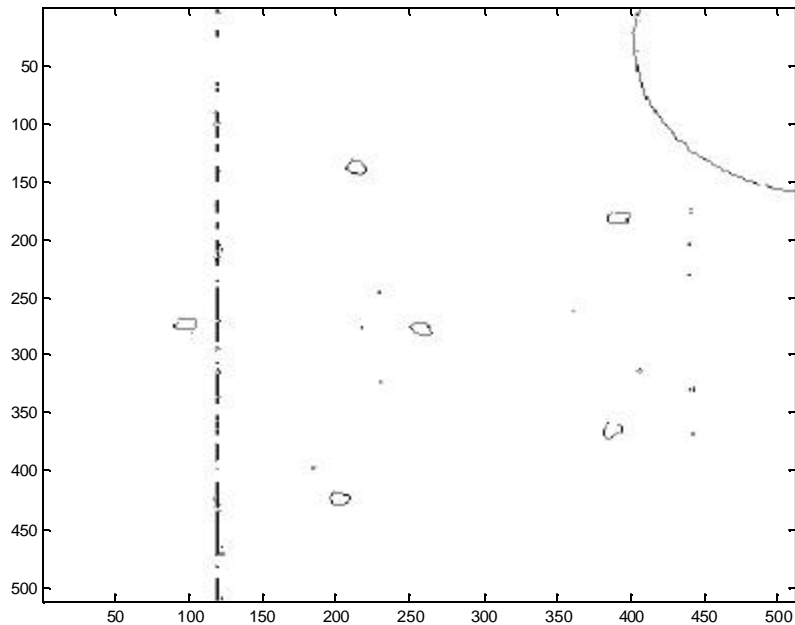
Figure 77 Edge detected post-processed High-dose (130 mRad) image using the Prewitt method.

3.4 Procedure for making comparisons

Quantitative comparison focuses on the disk and the specks produced by the ACR phantom. MATLAB possesses functions that aid in procuring data for analysis. IMSHOW displays an image as a MATLAB figure. PIXVAL "interactively displays the data values for pixels as you move the cursor over the image" (15:10-4). IMPIXEL "returns the data values for a selected pixel or set of pixels. You can supply the coordinates of the pixels as input arguments, or you select the pixels using a mouse" (15:10-4). HIST takes in data and displays them in the form of a histogram. MEAN calculates the mean of data and VAR calculates the variance of data.

The following procedure was used to obtain data for comparison for the unprocessed and processed images, focusing on the disk:

1) Using IMSHOW, the image is displayed as a figure.

66

2) PIXVAL is called to invoke MATLAB's real-time display of pixel coordinates and color data.

3) Using IMPIXEL, 30 distinct values within the disk are randomly chosen in a spiral fashion by using the mouse cursor in MATLAB, starting from the outside towards the center.

4) IMPIXEL is used again to randomly choose 30 distinctly separate values just outside the disk, again in a spiral fashion, starting close to the perimeter of the disk and going away from the disk.

5) Using MEAN and VAR, the mean and variance of the data inside the disk and just outside disk are found.

6) HIST is used to display the histogram of the data.

7) Using the mean and variance, the following Fisher ratio (FR) is calculated, where μ_1 and μ_2 are the mean of the disk data and mean of the background data, respectively, and s_1 and s_2 represent the variance of the disk data and the variance of the background data, respectively:

$$FR = \sqrt{\frac{\left(m_1 - m_2\right)^2}{s_1^2 + s_2^2}}$$

8) The FR's of the unprocessed and processed images for the disk are then compared.

The data for comparison that focuses on the specks is obtained with the following procedure:

1) Using IMSHOW, the image is displayed as a figure.

2) PIXVAL is called to invoke MATLAB's real-time display of pixel coordinates and color data.

3) Using IMPIXEL, 6 distinct values, one within each speck.

4) IMPIXEL is used again to randomly choose 6 distinctly separate values just outside each speck.

5) Using MEAN and VAR, the mean and variance of the data inside the specks and just outside specks is found.

6) HIST is used to display the histogram of the data.

7) Using the mean and variance, the Fisher ratio (FR) is calculated.

The FR's of the unprocessed and processed images for the specks are then compared.

A qualitative comparison was conducted by the WPAFB Radiology Department nuclear physicist, Lt Col William Ruck. Lt Col Ruck looked for three groups of microcalcifications, three groups of masses, and four fibers in the images. He was concerned with the possibility that the image processing may introduce artifacts that mimic abnormal pathology. Lt Col Ruck was also looking for any suppression of known features in the post-processed images as compared to the raw high-dose image obtained.

4. Results and Analysis

The goal of this research is to improve the quality of mammography images captured at a lower than typical dosage of X-rays using image processing techniques. To quantify how well the post-processing of the lower dose mammography images worked, the Fisher ratio was taken between the pixel intensities of the disk and the immediate

background surrounding the disk as well as pixel intensities of the six specks and their surroundings. The Fisher ratio is the ratio of the squared difference of the means over the sum of the variances, all square rooted. This ratio quantifies the separation between the disk data and the background data, as well as the separation between the speck data and the background data. The most important criterion in mammography images is contrast. Increasing the Fisher ratio between the disk and the background (as well as between the specks and the background) increases contrast. Figure 78 through 83 show the Fisher ratio results with various dose images for the disc. The histograms for the disk data and the background data were estimated using the MATLAB function HIST on the pixel data obtained using IMPIXEL. The mean and variance were obtained from the histogram data in order to calculate the Fisher ratio.

Figure 78 Histogram of 60 pixel values (30 inside and 30 just outside of the disk, chosen randomly using IMPIXEL) for the Very-low dose (50 mRad) image.

Figure 79 Histogram of 60 pixel values (30 inside and 30 just outside of the disk, chosen randomly using IMPIXEL) for the Low dose (100 mRad)

Figure 80 Histogram of 60 pixel values (30 inside and 30 just outside of the disk, chosen randomly using IMPIXEL) for the Low-medium dose (110 mRad)

Figure 81 Histogram of 60 pixel values (30 inside and 30 just outside of the disk, chosen randomly using IMPIXEL) for the Medium-high dose (120 mRad)

Figure 82 Histogram of 60 pixel values (30 inside and 30 just outside of the disk, chosen randomly using IMPIXEL) for the Medium-high dose (130 mRad).
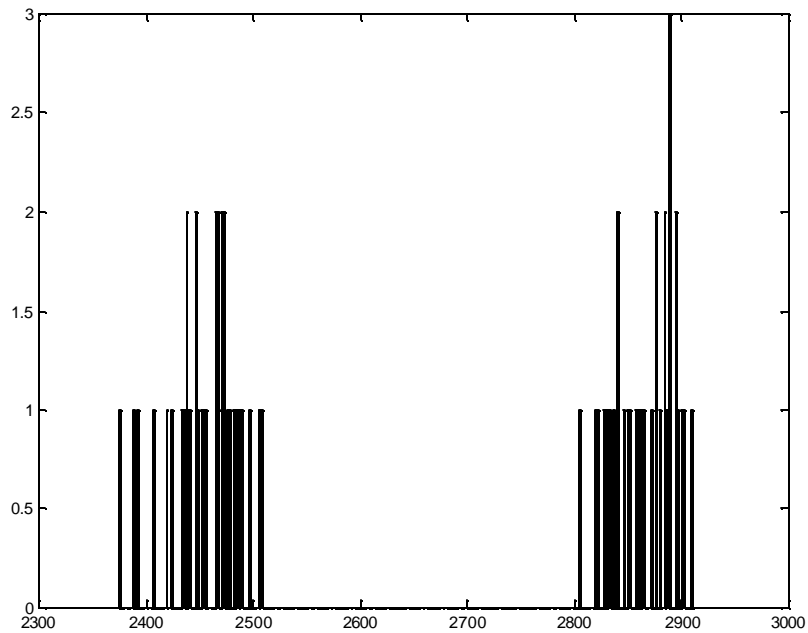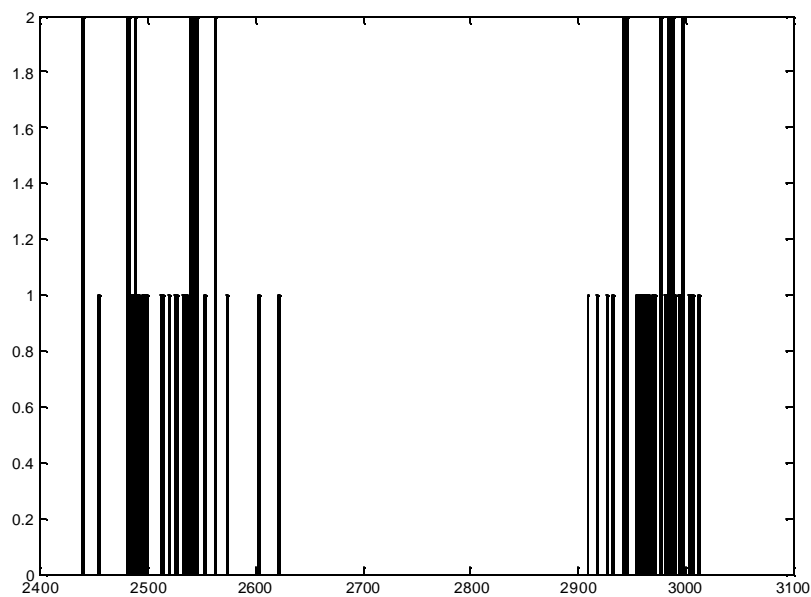
Figure 83 Histogram of 60 pixel values (30 inside and 30 just outside of the disk, chosen randomly using IMPIXEL) for the Very-high dose (150 mRad).

The Fisher ratio tends to increase as a function of X-ray dosage. As the X-ray dosage increases, the contrast of the image also increases, leading to higher Fisher ratios.   The Fisher ratio of the high dose image is 12.2. The goal is to improve the Fisher Ratio of the lower dose images to meet or exceed the Fisher ratio of the high dose image. The Figures 84 through 88 show the Fisher ratio results for the disk in post-processed images with various dosages.
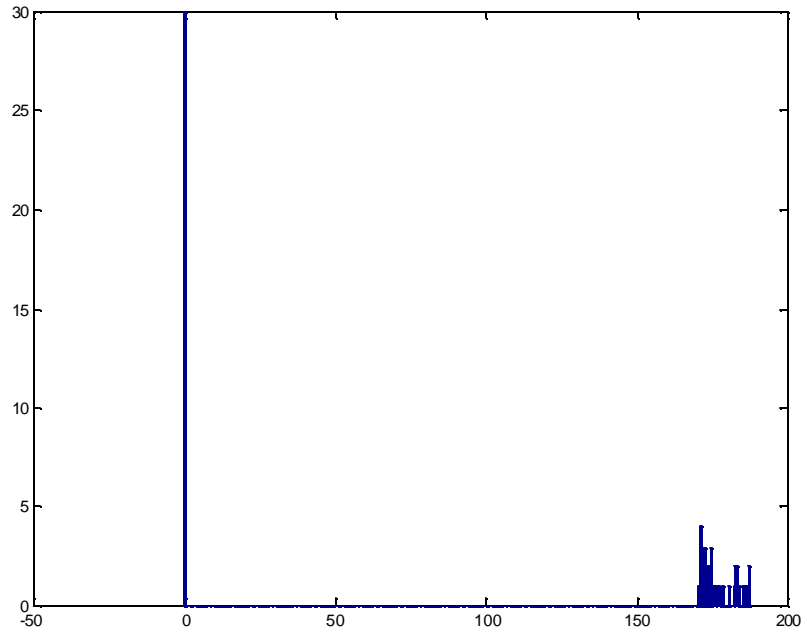
Figure 84 Histogram of 60 pixel values (30 inside and 30 just outside of the disk, chosen randomly using IMPIXEL) for the post-processed Very-low dose (50 mRad).
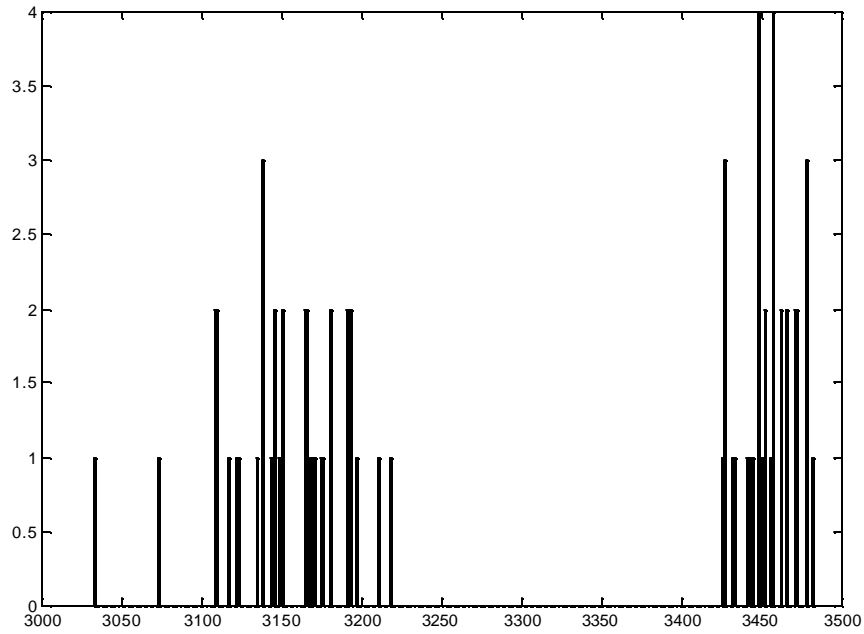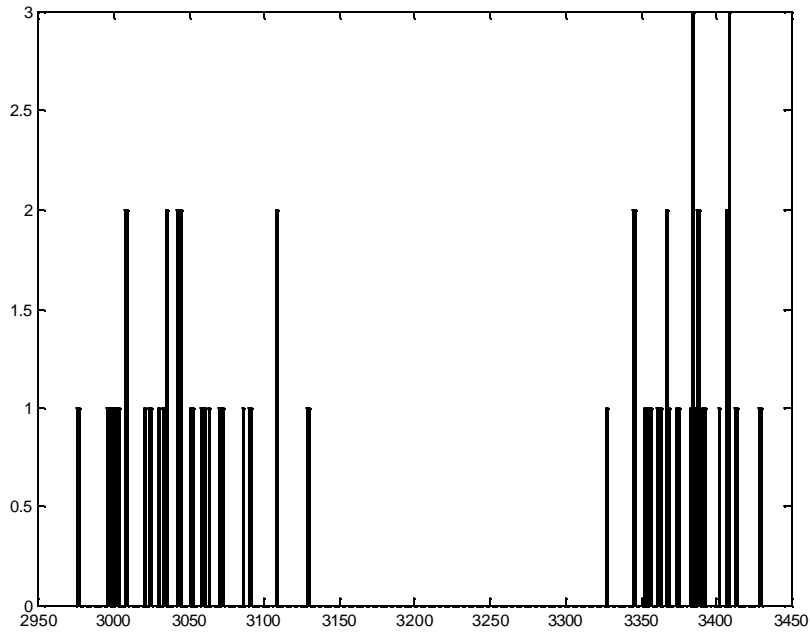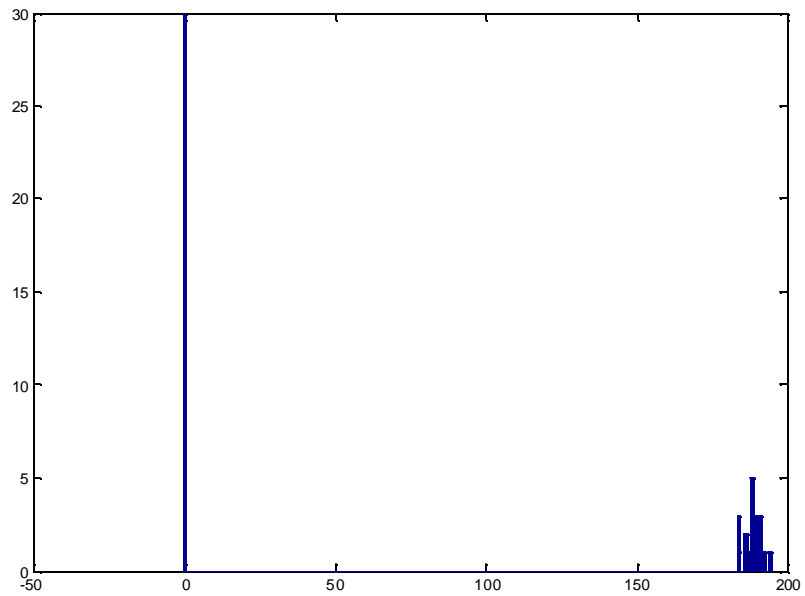

Figure 85 Histogram of 60 pixel values (30 inside and 30 just outside of the disk, chosen randomly using IMPIXEL) for the post-processed Low dose (100 mRad).
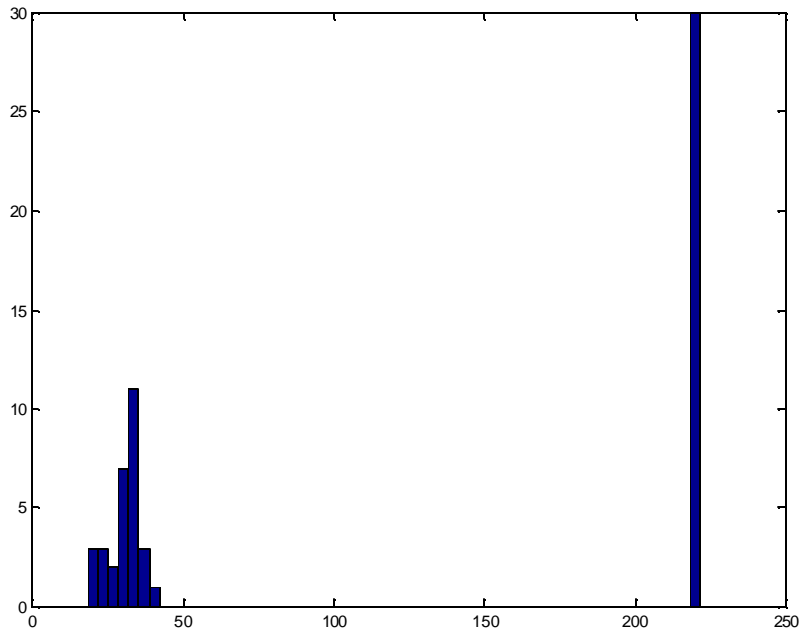
Figure 86 Histogram of 60 pixel values (30 inside and 30 just outside of the disk, chosen randomly using IMPIXEL) for the post-processed Low-medium dose (110 mRad).
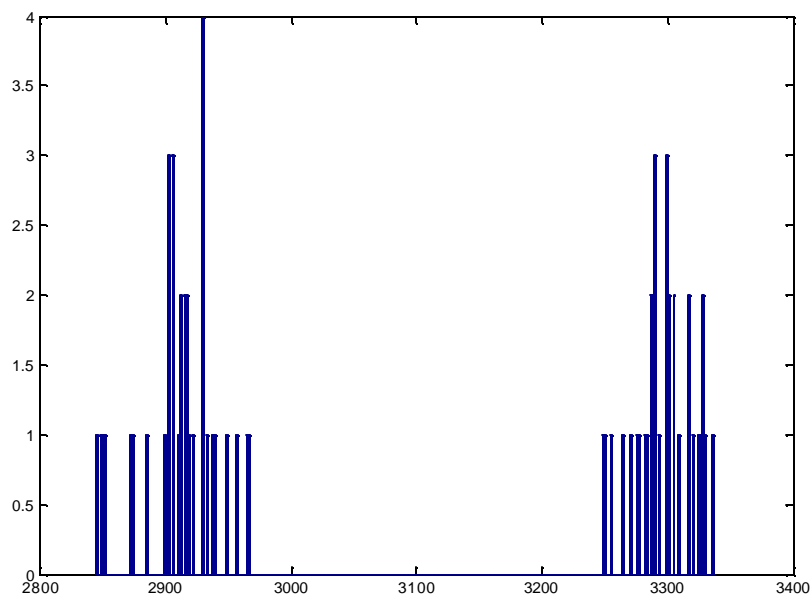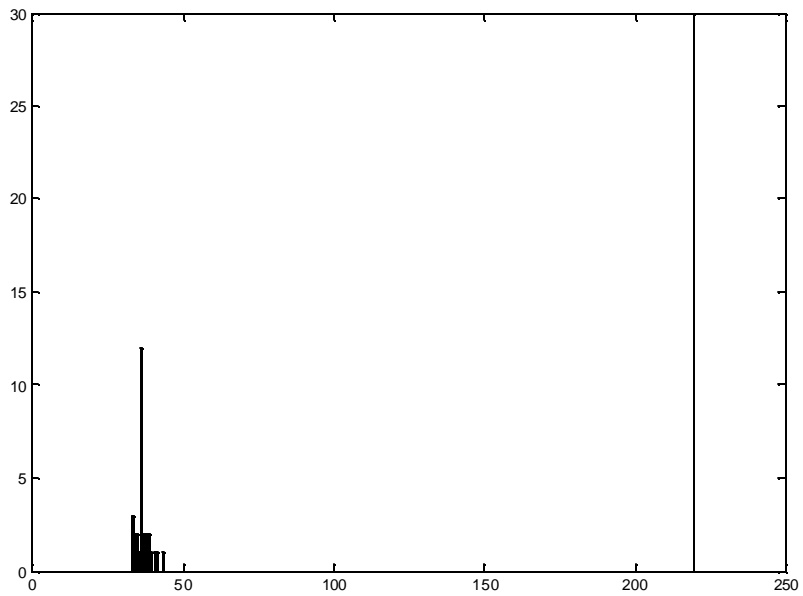

Figure 87 Histogram of 60 pixel values (30 inside and 30 just outside of the disk, chosen randomly using IMPIXEL) for the post-processed Medium-high dose (120 mRad).
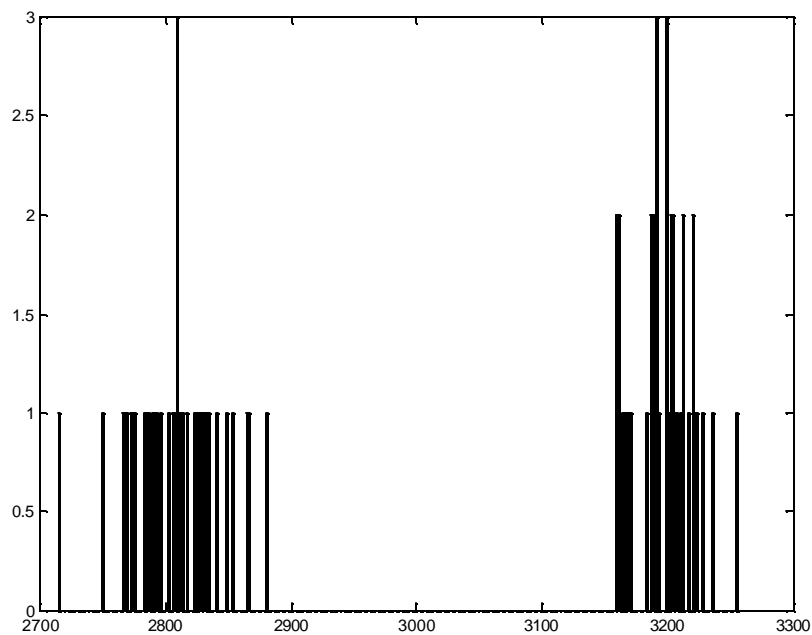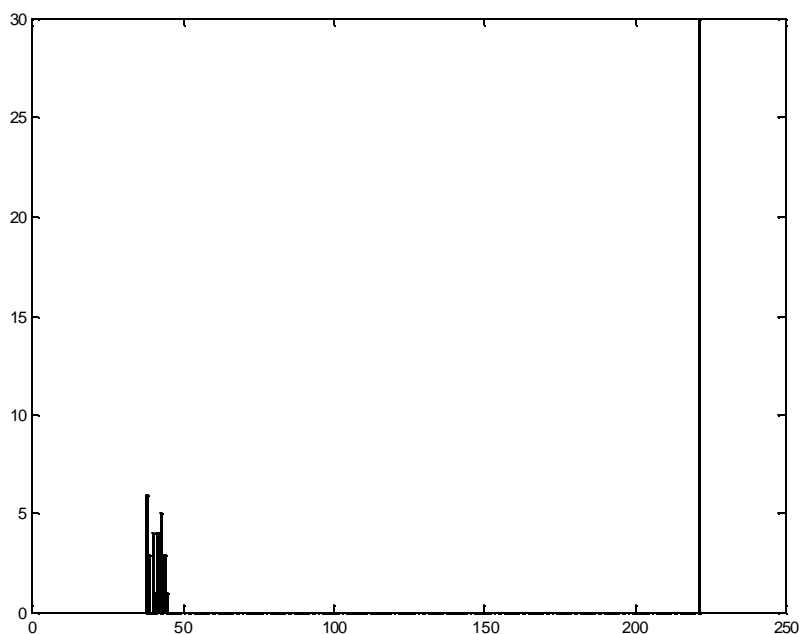
Figure 88 Histogram of 60 pixel values (30 inside and 30 just outside of the disk, chosen randomly using IMPIXEL) for the post-processed High dose (130 mRad).

Disk Fisher ratios (unprocessed)
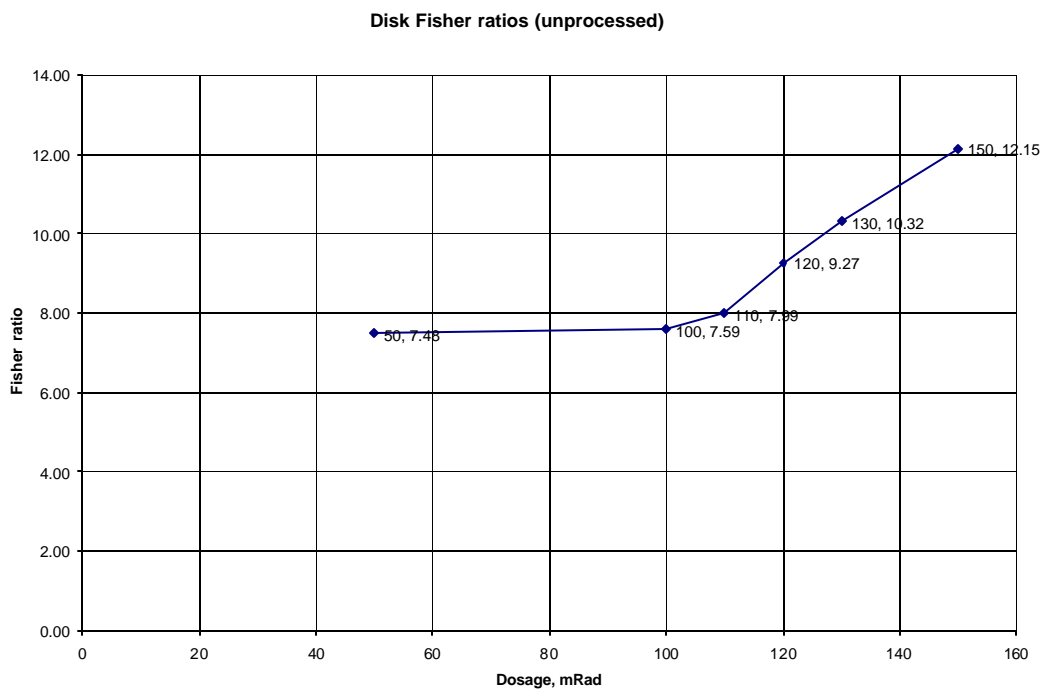
Figure 89 Comparison of Fisher ratios for the contrast of the disk and the background of the image for various doses of X-rays.

Disk Fisher ratios (post-processed)
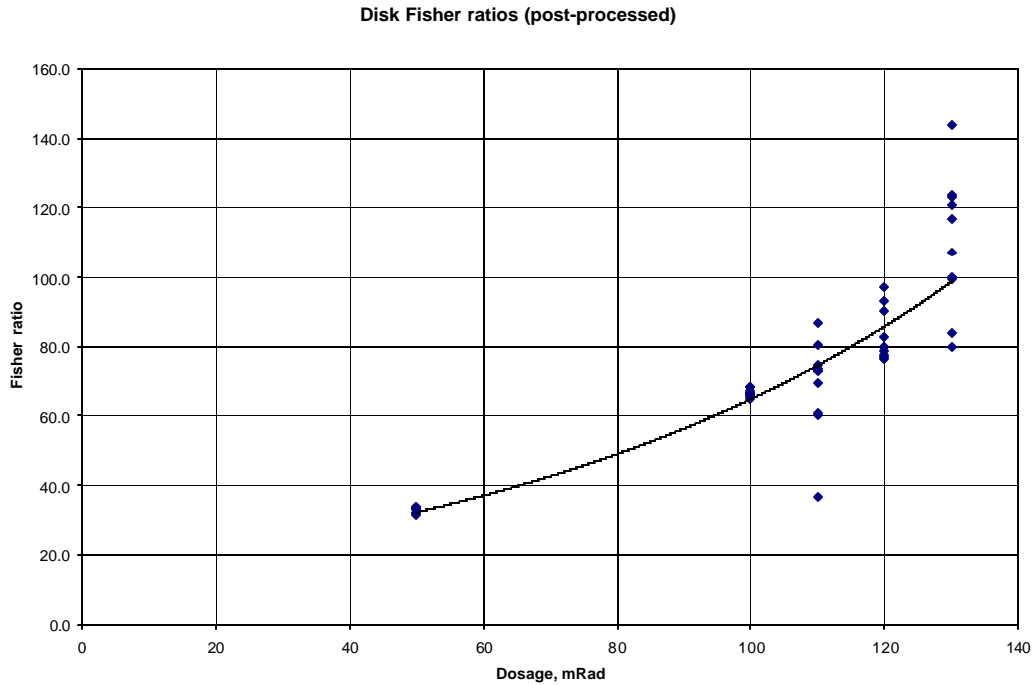
Figure 90 Comparison of Fisher ratio for the contrast of the disk and the background of the Post-processed image for various doses of X-rays.

The post-processed images possess Fisher ratios that are higher than the high dose image in terms of the distinguishing the disk from its background. Error is associated with the Fisher ratio results due to sampling variation (since only thirty disk and thirty background samples were employed). Regardless, the Fisher ratio trend for the lower dose images increases as expected.   Quantitatively, the post-processing achieves the goal of improving the image quality of the lower dose mammography images to exceed the high dose mammography image quality.

Figures 91 through 96 show the Fisher ratio results for the specks in images with various dosages.

Figure 91 Histogram of 12 pixel values (1 inside each of 6 specks and 1 just outside each of 6 specks, chosen randomly using IMPIXEL) of the Very-low dose (50 mRad) image.

Figure 92 Histogram of 12 pixel values (1 inside each of 6 specks and 1 just outside each of 6 specks, chosen randomly using IMPIXEL) of the Low dose (100 mRad) image.

Figure 93 Histogram of 12 pixel values (1 inside each of 6 specks and 1 just outside each of 6 specks, chosen randomly using IMPIXEL) of the Low-medium dose (110 mRad)

Figure 94 Histogram of 12 pixel values (1 inside each of 6 specks and 1 just outside each of 6 specks, chosen randomly using IMPIXEL) of the Medium-high dose (120 mRad) image.

Figure 95 Histogram of 12 pixel values (1 inside each of 6 specks and 1 just outside each of 6 specks, chosen randomly using IMPIXEL) of the High dose (130 mRad) image.
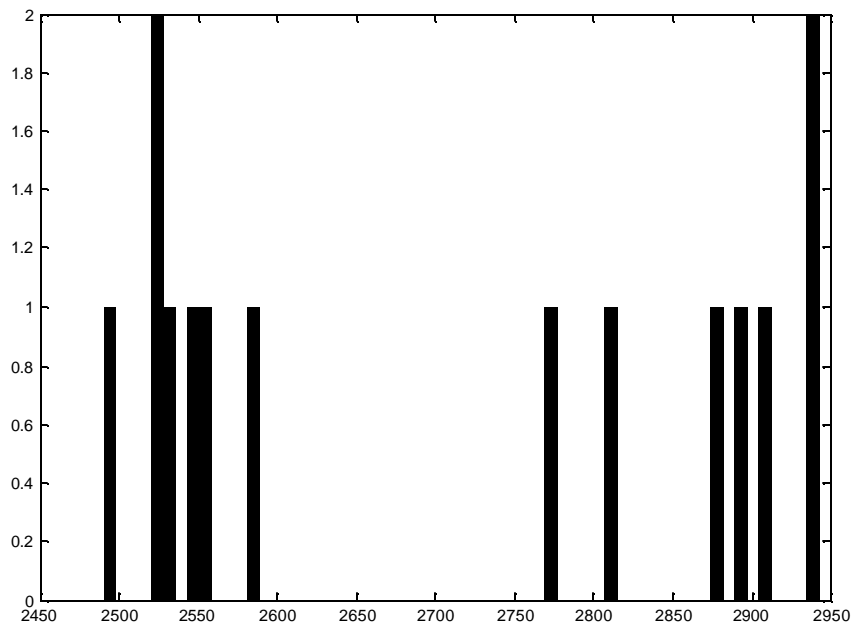
Figure 96 Histogram of 12 pixel values (1 inside each of 6 specks and 1 just outside each of 6 specks, chosen randomly using IMPIXEL) of the Very-high dose (150 mRad) image.

Figures 97 through 101 represent the Fisher ratio results for various post-processed dose images focusing on the specks.
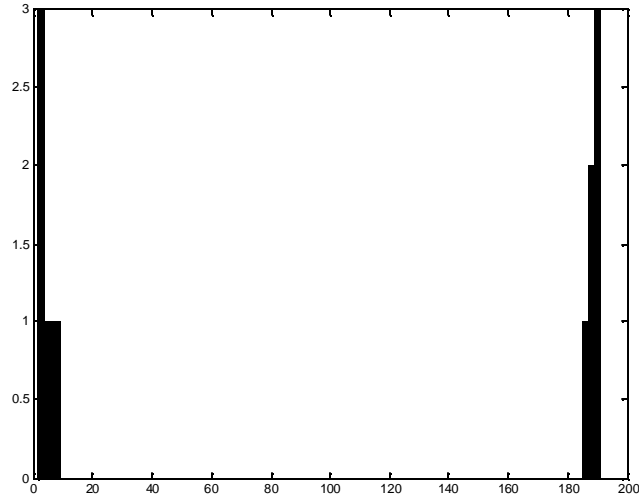
Figure 97 Histogram of 12 pixel values (1 inside each of 6 specks and 1 just outside each of 6 specks, chosen randomly using IMPIXEL) of the post-processed Very-low dose (50mRad) image.
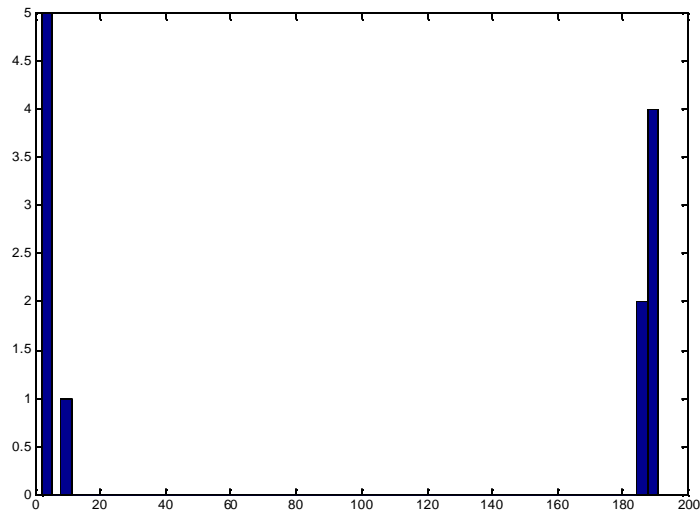
Figure 98 Histogram of 12 pixel values (1 inside each of 6 specks and 1 just outside each of 6 specks, chosen randomly using IMPIXEL) of the post-processed Low dose (100 mRad) image.
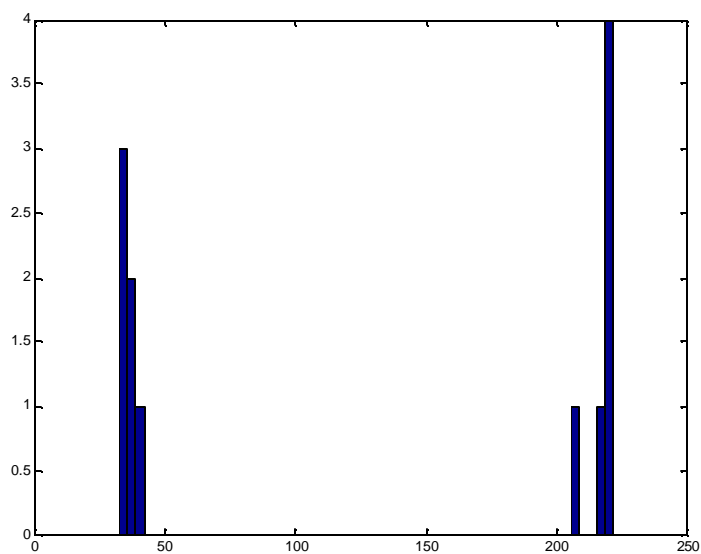
Figure 99 Histogram of 12 pixel values (1 inside each of 6 specks and 1 just outside each of 6 specks, chosen randomly using IMPIXEL) of the post-processed Low-medium dose (110 mRad) image.
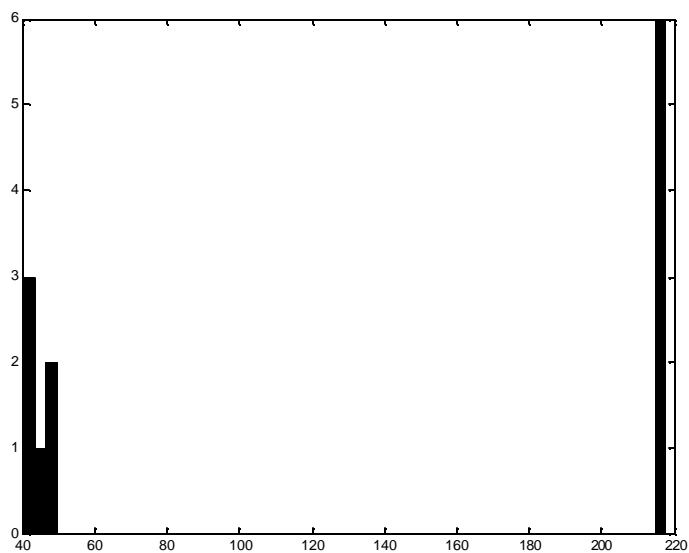
Figure 100 Histogram of 12 pixel values (1 inside each of 6 specks and 1 just outside each of 6 specks, chosen randomly using IMPIXEL) of the post-processed medium-high dose (120 mRad) image.
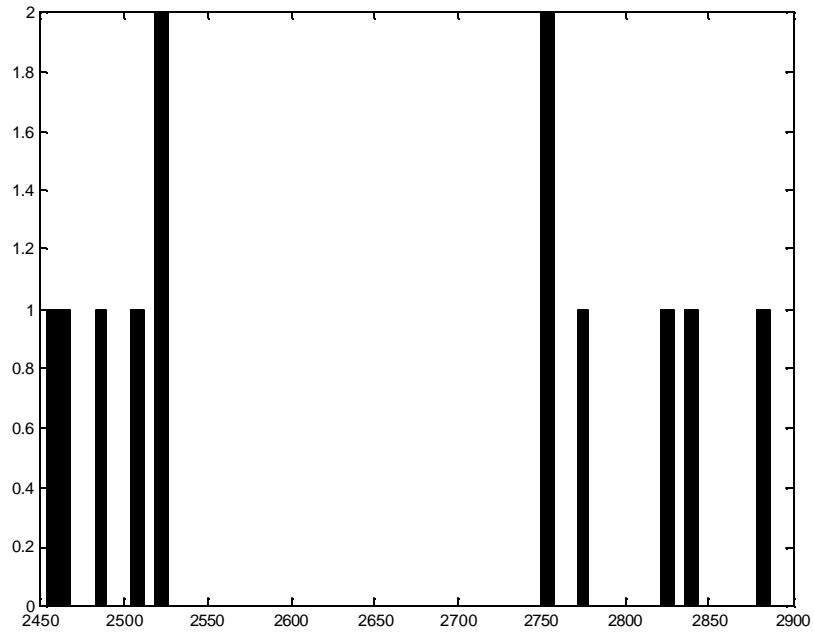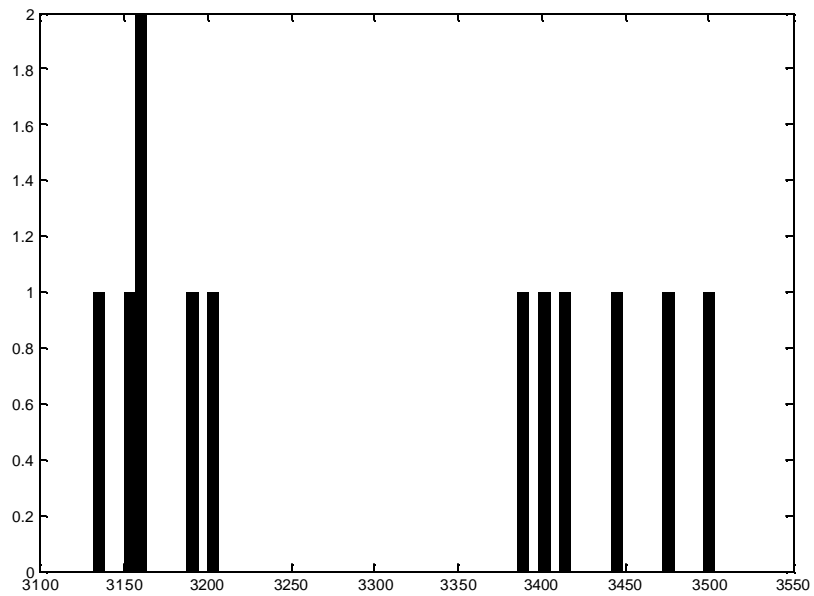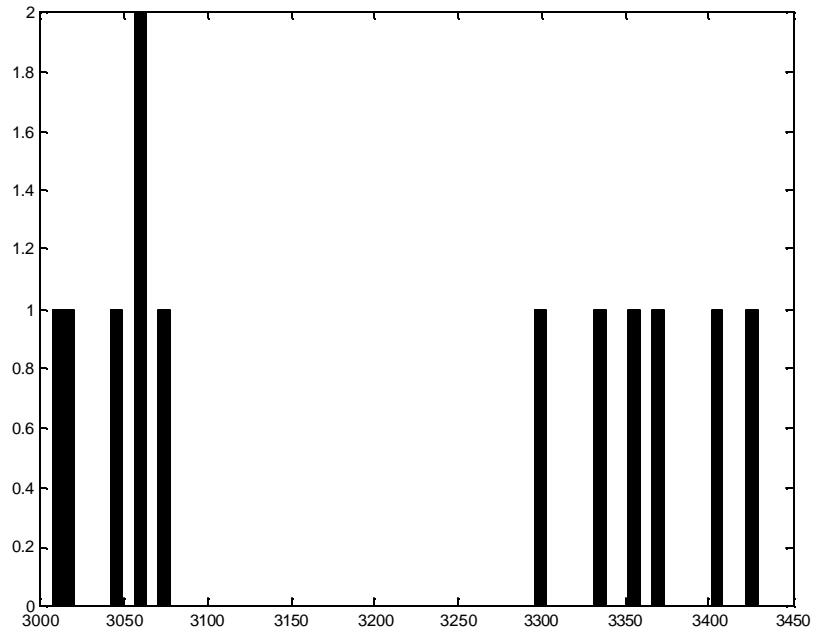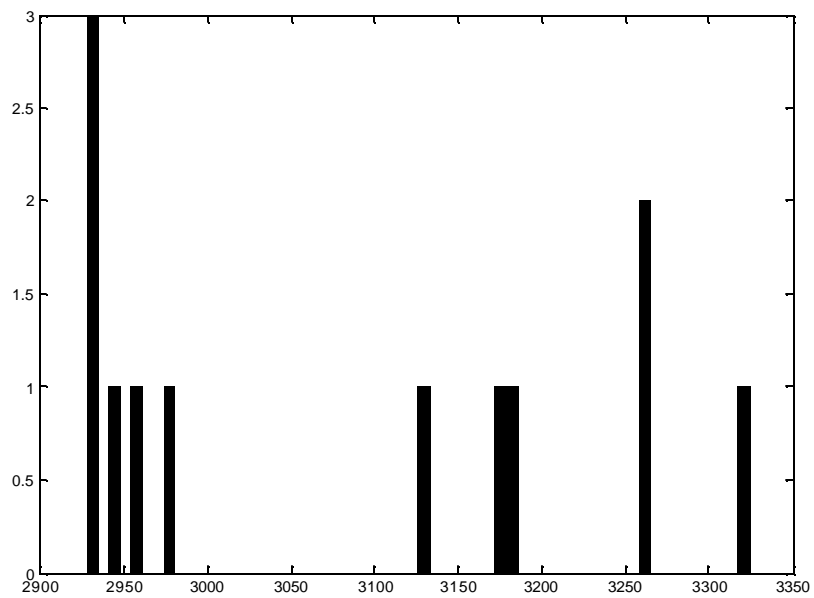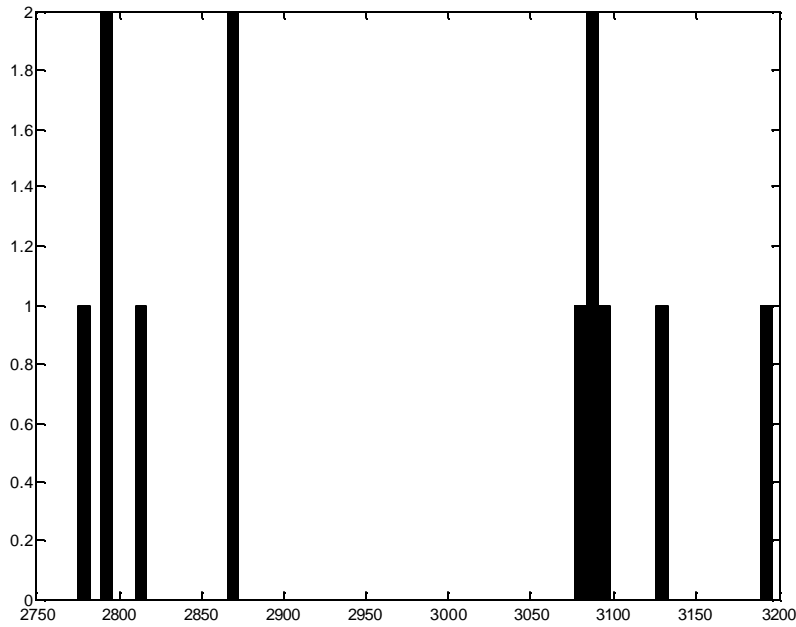
81
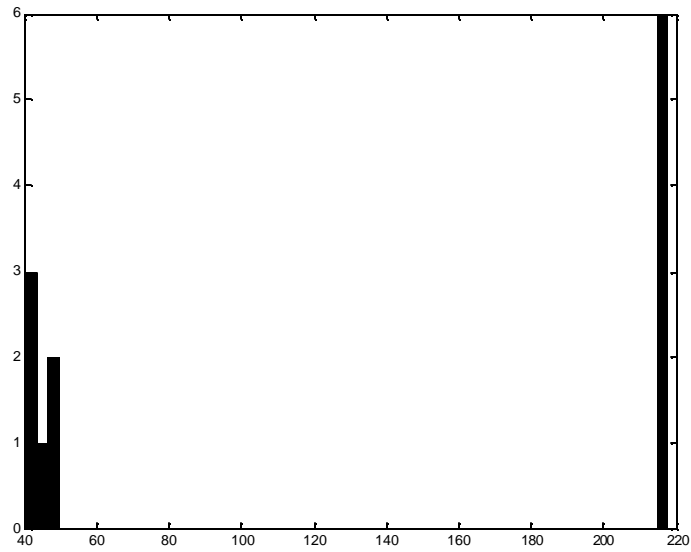
Figure 101 Histogram of 12 pixel values (1 inside each of 6 specks and 1 just outside each of 6 specks, chosen randomly using IMPIXEL) of the post-processed High dose (130 mRad) image.

Specks Fisher ratios (unprocessed)
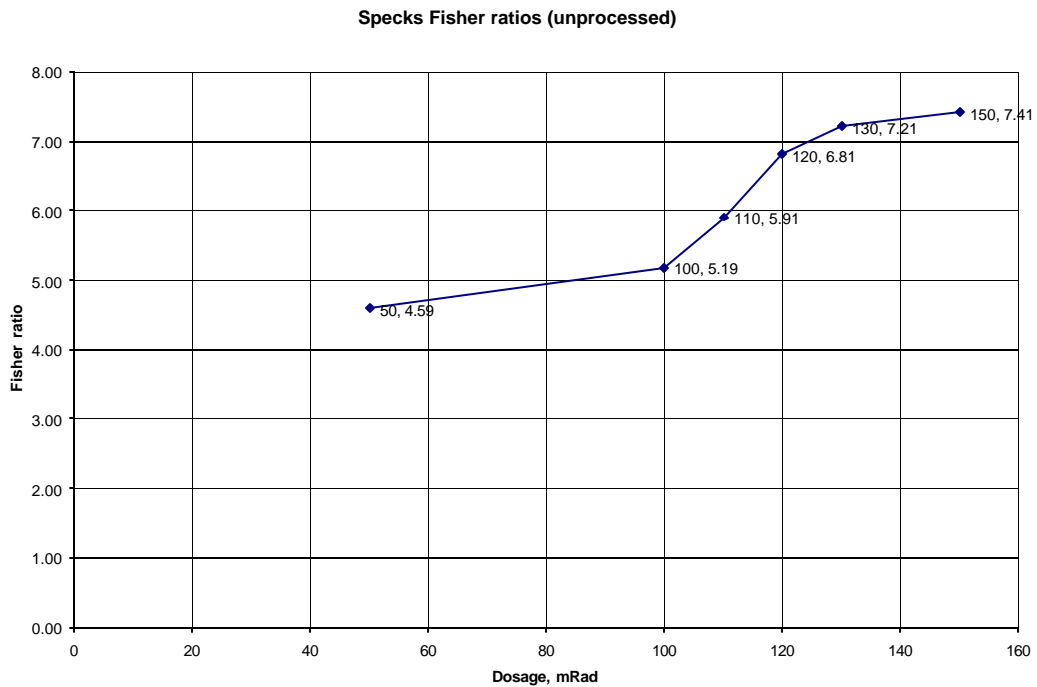
Figure 102 Comparison of Fisher ratio for the contrast of the specks and the background of the image for various doses of X-rays.

Specks Fisher ratio (post-processed)
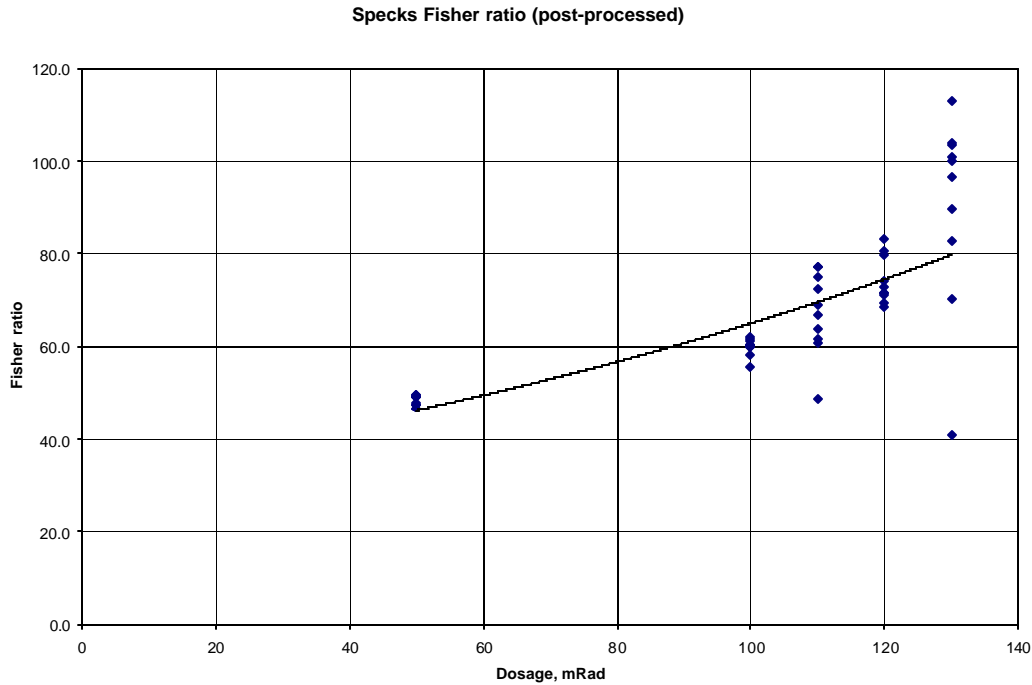
Figure 103 Comparison of Fisher ratio for the contrast of the specks and the background of the Post-processed image for various doses of X-rays.

The Fisher ratio for the specks and their background for the post-processed images are higher than their unprocessed counterparts and higher than that of the high dose image. This means that the contrast in the image when focusing on the specks improved as a result of the post-processing. The expected trend of increasing Fisher ratio as dosage increases for the post-processed images is apparent. Error due to the sampling variation introduced when randomly choosing the pixel values using IMPIXEL is apparent. However, the image quality based on the Fisher ratio results exceeds the image quality of the high dose image. Quantitatively, the results show that the post processed, lower dose mammography images exceed the image quality of the high dose image.

The qualitative comparison conducted by the WPAFB Radiology Department nuclear physicists Lt Col William Ruck shows promising success. Lt Col Ruck stated

that three masses and three groups of microcalcifications of differing diameters must be apparent to pass current ACR standards. Lt Col Ruck was still able to locate speck groups and the one mass (disk) group, which he thought was satisfactory for the research at hand. Lt Col Ruck also noticed some artifacts that are apparent in the post-processed edge-enhanced images. However, he stated those particular artifacts are not minute enough in diameter to be misconstrued as microcalcifications. Thus the expectation in improved-resolution post-processed mammography images for lower radiation doses was met.

5. Discussion

The results presented indicate that post processing to improve the image quality of low dose mammography images may aid in reducing X-ray exposure to patients. Quantitatively, the post processing improves the very-low, low , low-medium, medium-high, and high dose mammography images of the ACR phantom using uneven illumination correction, histogram equalization, denoising and edge detection.

Correction of uneven illumination is required due to the scattering effects of low dose X-rays. The low dose image possesses the highest degree of scattering among the images. The uneven illumination correction subtracts a coarse estimate of the very-low dose image to yield a sharpened image. The effect of scattering in the low dose image is significantly reduced after this processing. This effect is also reduced in the case of the low, low-medium, medium-high and high dose images. Although all scattering effects are not eradicated, the uneven illumination correction makes the lower dose images have

a background with an appearance that mimics the very-high dose image without introducing artifacts that interfere with the objects of interest, the disk and specks.

Histogram equalization dramatically enhanced the contrast in each of the lower dose images. The disk and specks in the very-low dose image are not easily discernable with the naked eye. However, the histogram equalization brings out the disk and the specks, due to the spreading of the histogram to a more uniform distribution. The same holds true for the low, low-medium, medium high, and high dose images, although these images were not degraded as severely as the very-low dose image as a result of varying X-ray exposures. Nonetheless, the low, low-medium, medium-high, and high dose images still benefited from the histogram equalization. In fact, the histogram equalized images possess a more uniform distribution of pixel values than the very-high dose image, meaning that the former have higher contrast than the latter.

Noise introduced during the procurement of the images is apparent in the lower dose images, however, the RDWT successfully denoises the images. In each case for the lower dose images, the RDWT filter reduced the Gaussian noise, as is apparent in the denoised images. To further test the performance of the filter, more additive Gaussian noise was added. The RDWT filter dramatically reduced the added noise in several iterations in the cases of the very-low, low, low-medium, medium-high, and high dose images.

The Fisher ratios for the post-processed lower dose mammography images exceeded that of the high dose image in the case of the disk samples. In the case of the speck samples, the Fisher ratios of the post-processed lower dose mammography images exceeded that of the high dose image. Two trends were expected from this research in

terms of the Fisher ratio. First, it was expected that the Fisher ratio would increase for the images captured at higher doses of X-rays. This is due to the assumption that the higher dose images have higher contrast, less scatter contribution, and less noise degradation. The results followed this trend. Secondly, the trend that the Fisher ratio would increase in the lower dose mammography images after post-processing was expected. The Fisher ratio trend increased in the case of the post-processed lower dose images concentrating on the disk. The Fisher ratio trend also increased in the case of the post-processed lower dose images concentrating on the specks.

5.1 Future research topics

A logical next step for this research is using actual mammography images that have known malignancies in order to further test the effectiveness of the post processing techniques on lower dose images. Mammography images can also be blended with ACR phantoms to provide for a simulation of malignant tissue within a more realistic setting. This will require more sophisticated image processing techniques to improve the contrast, reduce the effects of scatter, and denoise the actual mammography images since it has more clutter than the images used in the research at hand.

Further investigation into the advantages of using the RDWT should also be considered. The RDWT designed to include unsharp masking and denoising attributes is advantageous for the research at hand. Initial experimentation with the RDWT yielded promising results in the areas of enhancement and denoising.

Also, the Fisher ratio is a good quantitative metric of comparison to test the contrast improvement of the post-processed images, however, it does not take into

account the skewed nature of the histograms. A quantitative measure of the quality of the image that incorporates the skewed nature of the histograms presented should be used. This quantitative measure should take into account the third moment information of the data.

The experimental setup used to procure digitized mammography data was sufficient for the research at hand. However, it is recommended to use a digital mammography machine to obtain the mammography images for future research. This will eliminate steps in the image chain that may introduce noise and degradation experienced in the experimental setup. Examples of the degradation encountered that can be avoided using digital mammography is the JPEG compression used to save the data from the original experimental setup and the use of the imaging plate. Possibilities for improving the image quality of reduced dose mammography images should increase as image processing techniques progress.

Bibliography

1.	Aldroubi, Akram and Michael Unser. *Wavelets in Medicine and Biology*. New York: CRC Press, 1996.

2.	Bankman, Isaac. *Handbook of Medical Imaging, Processing and Analysis*. New York: Academic Press, 2000.

3.	Burrus, C.Sydney, Ramesh A. Gopinath and Haitao Guo. *Introduction to Wavelets and Wavelet Transforms.* New Jersey: Prentice Hall, 1998.

4.	Clarkson, Peter M. and Henry Stark. *Signal Processing Methods for Audio, Images and Telecommunications*. New York: Academic Press, 1995.

5.	Duda, Richard O., Peter E. Hart and David G. Stork. *Pattern Classification*. New York: John Wiley & Sons, Inc., 2001.

6.	Dondelinger, Robert E. and others. *Interventional Radiology*. New York: Thieme Medical Publishers, Inc., 1990.

7.	Dudgeon, Dan E. and Russel M. Mersereau. *Multidimensional Digital Signal Processing*. New Jersey: Prentice-Hall, Inc., 1984.

8.	"German cabinet recommends reduction in X-ray dosage." Reuters Health information article. n. pag. http://www.auntminnie.com. 15 March 2002.

9.	Gustafson, Steven. Class notes, EENG 620, Introduction to Statistical Pattern Recognition. Graduate School of Engineering and Management, Air Force Institute of Technology, Wright-Patterson AFB, OH, January 2002.

10.	Haus, Arthur G. and Martin J. Yaffe. *Syllabus: A Categorical Course in Physics, Technical Aspeckts of Breast Imaging*. Oak Brook, IL: RSNA Publications, 1993.

11.	Jain, Anil K. *Fundamentals of Digital Image Processing*. New Jersey: Prentice Hall, 1989.

12.	Lim, Jae S. *Two-dimensional Signal and Image Processing*. New Jersey: Prentice Hall PTR, 1990.

13.	"Mammography." Excerpt from Creighton University School of Medicine article. n. pag. http://medicine.creighton.edu/radiology/Mammography.html. 15 October 2001.

14.   MATLAB. Version 6.1. Computer software. MathWorks, Inc., Natick MA, 2001.

15.   McNicholas, Michelle and Stephanie Ryan. *Anatomy for Diagnostic Imaging*. Philadelphia: WB Saunders Company, Ltd., 1994.

16.   Parker, J. Anthony. *Image Reconstruction in Radiology*. Boston: CRC Press, 1990.

17.   "Questions and and Answers About Screening Mammograms." Excerpt from National Cancer Institute article. n. pag. http://cis.nci.nih.gov/fact/5_28.htm. 21 November 2000.

18.   Strang, Gilbert. *Linear Algebra and Its Applications*. Philadelphia: Saunders College Publishing, 1988.

19.   Sigmon, Kermit. *MATLAB Primer, Fifth Edition*. New York: CRC Press, 1998.

20.   *The American Heritage College Dictionary*. New York: Houghton Mifflin Company, 1993.

21.   Tike, Brenda. "European CT community works to cut pediatric radiation dose." Excerpt from article. n.pag. http://www.auntminnie.com. 2 April 2002.

22.   Coifman, R.R. and D.L. Donoho. "Translation-Invariant De-noising." Technical Report, Yale University and Stanford University.

Vita

      1Lt Jesung Kim graduated from L.V. Berkner High School in Richardson, Texas. He entered undergraduate studies at the United States Air Force Academy in Colorado Springs, Colorado where he graduated with a Bachelor of Science degree in Electrical Engineering in June 1999 and earned his commission.

      His first assignment is at the Aeronautical Systems Center, Reconnaissance Systems Program Office, Wright-Patterson AFB, Ohio, where he serves as a project engineer for the Advanced Projects Branch of the Sensors, Links and Ground Stations Division. In October 1999, he entered the Graduate School of Engineering and Management, Air Force Institute of Technology. Upon graduation, he will be assigned to the Space and Missiles Center, LAAFB, California.

REPORT DOCUMENTATION PAGE		*Form Approved* *OMB No. 074-0188*

The public reporting burden for this collection of information is estimated to average 1 hour per response, including the time for reviewing instructions, searching existing data sources, gathering and maintaining the data needed, and completing and reviewing the collection of information. Send comments regarding this burden estimate or any other aspect of the collection of information, including suggestions for reducing this burden to Department of Defense, Washington Headquarters Services, Directorate for Information Operations and Reports (0704-0188), 1215 Jefferson Davis Highway, Suite 1204, Arlington, VA 22202-4302. Respondents should be aware that notwithstanding any other provision of law, no person shall be subject to an penalty for failing to comply with a collection of information if it does not display a currently valid OMB control number.
PLEASE DO NOT RETURN YOUR FORM TO THE ABOVE ADDRESS.

1. REPORT DATE *(DD-MM-YYYY)* 29-07-2002	2. REPORT TYPE **Master's Thesis**	3. DATES COVERED *(From – To)* Oct 2001-Jul 2002

4. TITLE AND SUBTITLE POST-PROCESSING OF LOW DOSE MAMMOGRAPHY IMAGES	5a. CONTRACT NUMBER
	5b. GRANT NUMBER
	5c. PROGRAM ELEMENT NUMBER
6. AUTHOR(S) Kim, Jesung, First Lieutenant, USAF	5d. PROJECT NUMBER
	5e. TASK NUMBER
	5f. WORK UNIT NUMBER

7. PERFORMING ORGANIZATION NAMES(S) AND ADDRESS(S) Air Force Institute of Technology Graduate School of Engineering and Management (AFIT/EN) 2950 P Street, Building 640 WPAFB OH 45433-7765	8. PERFORMING ORGANIZATION REPORT NUMBER AFIT/GE/ENG/02-35

9. SPONSORING/MONITORING AGENCY NAME(S) AND ADDRESS(ES) Attn: William R. Ruck, Lt Col e-mail: William.Ruck@wpafb.af.mil 74 MDG/SGSXN 4881 Sugar Maple Drive WPAFB, OH 45433 (937) 257-4986	10. SPONSOR/MONITOR'S ACRONYM(S)
	11. SPONSOR/MONITOR'S REPORT NUMBER(S)

12. DISTRIBUTION/AVAILABILITY STATEMENT

APPROVED FOR PUBLIC RELEASE; DISTRIBUTION UNLIMITED.

13. SUPPLEMENTARY NOTES

14. ABSTRACT

In mammography, x-ray radiation is used in sufficient doses to be captured on film for cancer diagnosis. A problem lies in the inherent nature of x-rays to cause cancer. The resolution of the images obtained on film is directly related to the radiation dosage. Thus, a trade off between image quality and radiation exposure is necessary to ensure proper diagnosis without causing cancer. A possible solution is to decrease the dosage of radiation and improve the image quality of mammograms using post-processing methods applied to digitized film images. Image processing techniques that may improve the resolution of images captured at lower doses include crispening, denoising, histogram equalization, and pattern recognition methods. The Wright Patterson Air Force Base Hospital Radiology Department sponsored this research and provided digitized images of the American College of Radiology (ACR) phantom, which is a model for mammogram image quality and classification. Side by side comparisons were performed of high dose images and low-dose images post-processed using the methods mentioned. The result was improved-resolution mammography images for lower radiation doses. Thus, this research represents progress towards solving a problem that currently plagues mammography: exposure of patients to high doses of cancer-causing radiation to obtain quality mammography images. By improving the image quality of mammography images at lower radiation doses, the problem of cancer induced by high radiation exposure is alleviated.

15. SUBJECT TERMS
Mammography, Crispening, Denoising, Histogram equalization, Pattern recognition

16. SECURITY CLASSIFICATION OF:			17. LIMITATION OF ABSTRACT	18. NUMBER OF PAGES	19a. NAME OF RESPONSIBLE PERSON Steven C. Gustafson, ENG
a. REPORT	b. ABSTRACT	c. THIS PAGE	UU	92	19b. TELEPHONE NUMBER *(Include area code)* 785-3636 x4598
U	U	U			

Standard Form 298 (Rev. 8-98)
Prescribed by ANSI Std. Z39-18